This is to certify that the

thesis entitled

ACOUSTIC EMISSION ASSOCIATED WITH INTERFACIAL FAILURE OF CU-NI LAYERED COMPOSITES.

presented by

Motilal J. Tayal

has been accepted towards fulfillment
of the requirements for
M.S degree in Metallurgy

(Dr.K.Mukherjee) (Dr.F.Fink)
Major professor

Date November 13,1986.

ACOUSTIC EMISSION ASSOCIATED WITH INTERFACIAL FAILURE OF CU-NI LAYERED COMPOSITES

By

Motilal J. Tayal

A THESIS

Submitted to

Michigan State University

in partial fullfillment of the requirements

for the degree of

MASTER OF SCIENCE

Department of Metallurgy, Mechanics, and Materials Science

1986

ABSTRACT

ACOUSTIC EMISSION ASSOCIATED WITH INTERFACIAL FAILURE OF CU-NI LAYERED COMPOSITES

By

Motilal J. Tayal

Two kinds of Cu-Ni metallic composites were made, symmetric (Cu-Ni-Cu) and asmmetric(Cu-Ni). The properties of the interface were varied by varying the diffusion zone and by introducing artificial defects (voids) at the interface. Acoustic emission, during tension test of these composites, was used to characterise interface cracking. It was found that acoustic emission activity during loading starts very early in the presence of a bad bond in these composites. At any given load the number of cumulative AE counts is higher for a bad bond than for a good bond. The total number of AE counts during tension was found to increase with an increase in the size of the defects present at the interface.

ACKNOWLEDGEMENTS

I would like to take this opportunity to thank Dr. Kalinath Mukherjee and Dr. Fred Fink for their constant support and guidance during this research. Without their encouragement and help this work would have been far from reality. I would like to thank Dr. N.J. Altiero and my friend Mr. Y.H. Youn for helping me in tackling the mechnanics part of the this research. I would also like to thank the Centre for Composite Materials and Structures for financial support for this research. Last but not the least, I would like to thank my friends and my colleagues, especially Mr. S. Sircar and Mr. H. Kim, for their timely help and support when I needed them most.

TABLE OF CONTENTS

LIST OF FIGURES

LIST OF TABLES

I. INTRODUCTION

Composite materials are gaining popularity in engineering applications due to their flexibility in allowing achievement of desired mechanical and other physical properties in combination with light weight components. Composite materials are widely used these days in industries like auto, aerospace manufacturing, nuclear plants and chemicals manufacturing [1]. Metallic composites consist of layers of dissimilar metals or alloys, metallurgically bonded together. It is an extension of the current clad metal technology. Current examples of engineering applications of clad metal [2] include zircaloy cladding of fuel rods for the nuclear industry, stainless steel overlay of pressure vessel, for the nuclear and refinery industry [3] cladding of power transmission lines for the utility industry and the cladding of ship hulls for corrosion resistance.

A potentially important application area for clad metal is the automotive industry. Current applications are limited primarily to decorative trim. Howerver with new requirments for fuel efficiency and safety, opportunities exist for structural applications as well. For example the feasibility of a stainless steel clad aluminum bumper has been demonstrated by Texas instruments [4]. This clearly provides a weight reduction for comparable strength.

Before putting these kinds of composites to use, it is important to understand the basic behavior of such materials when subjected to

service loads. To determine the mechanical response of such composites we need to consider the following points:

(a) The nature of the interface and the ways the structure of the interface varies with heat-treatment.

(b) Types of defects present at the interface and the effect of these flaws on the mechanical response, and in particular the potential for delamination of the clad material.

For the present study, a Cu-Ni composite was chosen (there was no specific reason for this choice except that Cu-Ni alloy systems form a complete range of solid solutions). The mechanical response of such a material to tensile loads, with varying properties at the interface were studied. Acoustic emission, during tensile testing, was used to investigate interface cracking. The properties of the interface were varied by varying the diffusion zone and by introducing artificial defects (voids) at the interface. The interface was tested qualitatively for defects, by using pulse-echo ultrasonic techniques. Finally the acoustic and mechanical response of the composite was correlated to the properties of the interface by computer.

II. LITERATURE SURVEY

2.1 Metallic Composites.

The possibility of a metallic composite with very high strength and ductility was proposed by Koehler [5]. The proposed material has a laminate structure of multiple layer films composed of two kinds of material with such a thickness that Frank-Read sources cannot operate inside. Koehler's model for composites required that individual layers be of the order of 100 atomic layers thick or less. Also it requires that one of the component materials of the composite has higher dislocation-line energy than the other one. When the dislocation-line energies are mismatched the termination of the motion of dislocation in one metal (low dislocation-line energy) is energetically favored over a dislocation propagation across the interface into the other metal (higher dislocation-line enegy).

Lehoczky [6] used the Al-Cu laminate to verify Koehler's model. He tested composites with varying layer thicknesses ranging from 1000 nm to 20 nm. Strengthening with decreasing layer thickness showed the validity of Koehler's model (Fig 1). Tensile properties of Ni/Cu(001)Ni triple layer films and single crystal films of (001)Cu and (001)Ni were studied by Yoshi and Takagi [7]. The yield stresses of composite films were found to be 2.5 to 5 times higher than those of Cu or Ni single crystal films, and were also higher than the values given by the mixture rule for Cu-Ni single crystal films (Fig 2). In the case of thick layers the dislocations generated in either

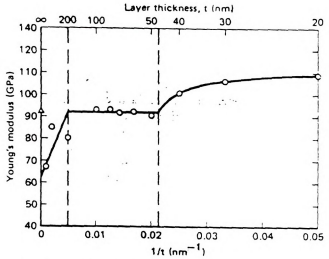

FIG.1. Dependence of average value of Young's modulus on inverse layer thickness.The Al and Cu layer thickness were equal in each laminate.

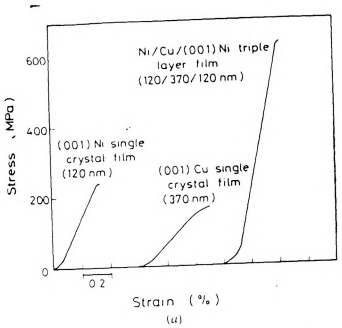

FIG.2. Typical stress-strain curves of (001)Ni, (001)Cu, and Ni/Cu/(001)Ni films. T.S direction is [001].

component of the composite will pile up in layers of one component (with lower dislocation-line energy) at the interface and therby provide the stress concentration needed for premature yield.

Different metallurgical composites with thick layers have been used in the past for various applications. Stainless steel cladded mild steel has been used as corrossion resistant material [8]. Stainless steel clad is generally available as plates and coils. Both single and double clad are available; However in the case of plate single clad is more common. Stainless steel clad plates find use in a number of major industries such as chemical processing, oil refining and food processing. The amount of cladding, expressed as a percentage of the total thickness of the plate, is available in thickness from 5 to 50 percent. The most widely used thickness of the clad are 10 and 20 percent.

Stainless steel clad aluminum combines the cleanability, stain-resistance, and toughness of stainless steel with the lightness and excellent heat-treatment characteristics of aluminum. Stainless steel clad copper finds its use in the electrial field because of its good electrical properties and heat transfer characteristics. Monel-clad steel is useful for heat-transfer equipment used in coastal area. Examples include the evaporators serving saline water plants and tube sheets of heat exchangers used in power stations, chemical plants and oil refineries. This clad is also used to handle the brines from salt wells of inland caustic-chlorine plants. 70/30 Cupro-Nickel clad steels are extensively used for tube sheets of condensers and heat exchangers where sea water or brakish water is the coolant. Their antifouling properties are particularly useful in sea water applications.

2.2 Manufacturing techniques for Composites.

Various methods of producing clad material have been used in the past. One of these consisted of placing two cladding metal plates that had been welded together in an ingot mold. Molten base metal was then cast around the plates. The solidified mass was then hot rolled to a convenient thickness and the welded area of the cladding metal plates cut away. This then provided two single clad plates. Double clad that is a symmetrical composite was produced similarly except that the cladding metal plates were previously positioned in an ingot mold and molten core metal poured between them.

Another method employed a pack assembly. To produce single clad material by this method two plates of cladding metal are placed together. A parting compound is placed between the faces of the plates to prevent bonding. Plates of the base metal are placed on the exposed side of the cladding metal. The edges of the pack are then welded for two reasons. Welding tends to minimize oxidation of surfaces to be bonded and keeps the various components in proper register during further processing. After welding, the assembly is heated and hot rolled sufficiently to achieve a bond. Once this has been done, the welded edges can be removed and the resultant single clad material further reduced to finish gage.

A different type of technique which is used for producing clad materials employs explosives [19]. With this technique the clad metal is held at a controlled distance from the base metal and the explosive charge detonated. This brings the surfaces to be bonded into intimate

contact and bonding is achieved. It is not necessary to heat the materials prior to bonding with this techniques.

The overlay welding method of cladding has recently gained commercial acceptance. Automatic welding methods are usually used to deposit two or more layers of cladding materials. A similar method uses a powder of cladding metal placed on the base metal slab and the powder is melted and fused to the surface of the slab (base metal) by an electric arc. Four ways to deposite stainless overlays [3] are shown in Fig 3. Stainless overlays are used in the pressure vessels built for the nuclear and refinery.

One other method which is worth refering to is Texas Instruments's continuous cold-bonding technique [4]. In this process the required layers of strip are rolled to correct gauge, super cleaned at special cleaning stations, then fed simultaneously into a heavy reduction mill where they are pressed together. The specially cleaned metal surfaces have an attraction for each other and the metals actually insterstice under pressure. After rolling, the material is sintered in special furnace to enhance the bond and further improve its integrity.

For producing thin film metallic composite two techniques have been used. The first is vacuum evaporation [9]. This technique consist of evaporating alternate layers of the components onto a common substrate. This technique has been used to obtain composition modulated films with enhanced elastic modulus, magnetization and super conductivity. Another method that has been used, is the electroplating

of alternate layers as described by Blum [10] in 1921. Electroplated layered composite can be obtained by either plating alternately from separte electrolytes of the two components or plating from a single electrolyte by switching the current density between two widely separated values. Cohen and Koch [9] use a similar technique for producing laminated composites of cyclic multilayered alloy (CMA) electrodeposits. The CMA technique was demonstrated by plating a wide variety of Ag-Pd CMA structures.

2.3 Pure Cu and Pure Ni studies.

Henning, Boswell and Corbett [11, 12] worked with polycrystalline Cu, Ni thin films (5000-20000 Å). Cu, Ni specimens were prepared by vacuum depostion of Cu and Ni on glass or NaCl substrates. They determined the mechanical behaviour of vapor deposited Cu and Ni. Tensile parameters for polycrystalline Cu, Ni films published by them is shown in Table 1. Tensile parameters for bulk Cu and Ni are also included in Table 1.

2.4 Rule of mixtures.

In the past, the rule of mixtures (an average of component properties weighted by cross sectional area fractions) has been used to characterize mechanical properties of clad material [13, 14]. The rule of mixtures model is illustrated in Fig 4. The figure shows a symmetrical composite with two components, " m" represents the base

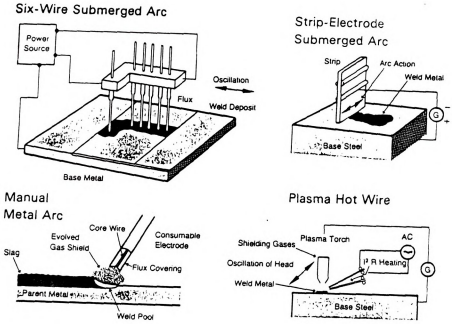

FIG.3. Four ways to deposit stainless overlays.

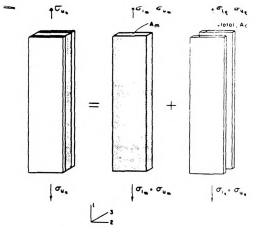

FIG.4. Rule of mixtures model for clad sheet material.

TABLE 1

Tensile parameters of CU AND NI films [11,2]

material	$t \times 10^{-3}$ (A^0)	σ_b (kg/mm^2)	σ_a (kg/mm^2)	$\epsilon_p \times 10^2$ (%)	$E \times 10^{-6}$ (psi)
Cu	20	50.6(51.5)	8.0(8.3)	23.8	24.89
Cu	20*	16.1 (18.7)	9.1(10)	27.0	28.01
Cu	3	46.9 (57.2)	8.0(9.9)	32.0	26.44
Ni	20	115 (154)	35.5(40)	5	17.49
Ni	20**	69 (76.5)	32.2(42)	14	8.11
Ni	2	114 (141)	35.7(40)	60	13.8
Ni(annealed) bulk		38.68-56.23	10.54-21	-	31
Cu(annealed) bulk		20.4-25.5	-	-	17

Film thickness= t, Elastic modulus= E, Breaking stress = σ_b , yield stress = σ_a , Plastic strain at fracture = ϵ_p , Average values are listed with maximum values in brackets.

* Annealed at 500^0 C for 30 min in 10^{-5} torr vacuum

** Annealed at 600^0 C for 1 hr in 10^{-5} torr vacuum.

metal (core) and "c" represents the cladding metal. The rule of mixtures is based upon the following assumptions:

(a) Bending stresses are negligible.

(b) The components of the composite deform together. There is no slipping of one component relative to the other at the interface.

(c) Material property differences between the composites' components induce no transverse stresses.

But if two sheet materials with different normal plastic anisotropies are pulled in uniaxial tension to the same elongation, the width and thickness strains which each experience will not be the same. When these two sheet materials, in turn are bonded together to form a composite, and then pulled, the necessity for strain compatibility would cause width and thickness stresses to be induced. For thin composite plate, straining uniformly, thickness stresses (σ_3) are probably negligible, but sizeable width direction stress might be induced. Considering these factors the modified isostrain model for uniaxial tensil deformation of clad sheet material is shown in Fig 5.

This characterization of the mechanical properties of clad materials is only useful when the bonding between the component metals is ideally perfect, otherwise the interface becomes the most favourable site for failure such as crack initiation and propagation, which might be a primary mode of composite failure. That is, the integrity of the cladding protection could be lost by delamination at the interface of the composite.

2.5 Interface characterisation.

Quantitatively defining the physical properties of the interfacial zone is very difficult due to the potential gradients in material properties and the smallness of the zone. Qualitatively, the interfacial zone can be characterised by (a) chemical composition of the interface; (b) various flaws present in the interfacial zone eg. voids, inclusions, cracks, etc.

In a Cu-Ni system there is complete solid solubility of the two metals, so no complication arise because of the possibility of intermediate or intermetallic compound at the interface. Only the composition profile of Cu-Ni has to be determined across the interface. In the past, concentration profiles have been measured by Auger electron spectroscopy and Electron microprobe. But neither of these gives a non destructive monitoring of changing profile (due to annealing). A method has recently been developed whereby interface concentration profile can be monitored sensitively and in-situ by measurement of contact resistance [14]. Correlation of changes in electrical resistance with changes in the concentration profile have been shown by Johnson & Bauer [14].

(a) Composition profile.

For theoretical determination of the composition profile from interdiffusion coefficient (D), it is necessary to solve the Fick's second law using boundary conditions which best describe the composite [15]. Since D is a function of composition, it is necessary to solve the following nonlinear partial differential equation:

$$(\partial c/\partial t) = (\partial/\partial y)[D\ (\partial c/\partial y)] \qquad \ldots(1)$$

if it can be assumed that the system is double infinite in y, the composition profile can be obtained by making use of the Boltzmann transformation

$$\eta = y/\ (2t^{1/2}) \qquad \ldots(2)$$

The Boltzmann transformation reduces equation 1 to an ordinary differential equation

$$-2\eta\ (dc/d\eta) = (d/d\eta)[D\ (dc/d\eta)] \qquad \ldots(3)$$

With the boundary conditions

$C = 1$ (pure Ni) for $\eta \rightarrow \alpha$

$C = 0$ (pure Cu) for $\eta \rightarrow \alpha$

equation 3 can be written in the form

$$-2\eta/D = d/d\eta\{\ln[D\ (dc/d\eta)]\} \qquad \ldots(4)$$

Integration gives

$$\ln\ (D\frac{dc}{d\eta}) - \ln A = -\int_{\alpha}^{\eta} \frac{2\eta'}{D}\, d\eta' ,$$

Where η' is a dummy variable and A is a constant of integration. Rewriting the preceding equation

$$D\frac{dc}{d\eta} = A \exp\ (-\int_{\alpha}^{\eta} \frac{2\eta}{D}\, d\eta') \qquad \ldots(5)$$

If equation 5 is integrated again and A is evaluated to fit the boundary conditions, then

$$C\ (\eta) = 1 - (\int_{\alpha}^{\eta} D^{-1} \exp\ (-\int_{\alpha}^{\eta} \frac{2\eta'}{D} d\eta')d\eta'\ (/\ (\int_{\alpha}^{+\alpha} D^{-1} \times$$

$$\exp\left(-\int_{\alpha}^{\eta} \frac{2\eta'}{D} d\eta'\right) d\eta' \quad (\qquad \ldots (6)$$

In order to solve equation 6 , it is necessary to proceed with an iterative approach. One begins this procedure knowing D(c) from experiment and assuming a first approximation to C (η). A good first approximation to the composition profile is

$$C(\eta) = \left(1-\mathrm{erf}(\eta/\langle D\rangle^{1/2}\right) \quad (, \qquad \ldots (7)$$

where $\langle D\rangle^{1/2}$ is the average interdiffusion coefficient and the error function is defined by

$$\mathrm{erf}(z) = \frac{2}{(\pi)^{1/2}} \left(\int_{0}^{z} \exp(-\eta^{2}) d\eta\right) .$$

The calculation of C(η) from equation 6 had been programmed for an IBM 360 computer by Tenney and Carpenter [15]. Values of $z=\eta/\langle D\rangle^{1/2}$ ranging from -3.5 to +3.5 were chosen in steps of 0.1. The iteration can be carried out as follows:

(1) Determine a set of C values from the z (or y) values and equation (7)

(2) With known D(c) values, evaluate an improved set of C(η) values using equation (6) [18].

(3) Using c values obtained from equation 6 redetermine D(c) for the new positions y and recalculate c from equation (6)

(4) Continue the iteration until two successive approximation are within the desired accuracy.

(b) Flaws in the interfacial zone.

The effect of defects like voids, inclusions and cracks etc. have been analysed for the non-metal composites [16]. Various complicated equations have been developed to predict the mechanical response of non-metallic composite material with various defects at the interface. Although not much information is available on the mechanical response of metallic composite with such defects, it is quite evident that these defects at the interface of such composites concentrate stresses and strains. Size and shape of the defect is also very important, because stress intensity factors depend on type of loading, geometry of sample and the shape and size of defect.

2.6 Acoustic Emission

The use of acoustic emission to characterize and evaluate an engineering structure under load is drawing much interest in the scientific and engineering communities. It is one of the first nondestructive testing methods to provide a means of evaluating structural integrity by the detection of active flaws that may ultimately cause failure of the material or structure. Sources of AE which generate stress waves in material include local dynamic movements, such as the initiation and propagation of cracks [20], twinning, slip or plastic deformation, sudden reorientation of grain boundaries [21], or martensitic phase transformation [22]. The stresses in a metallic system may be well below the elastic design limit, and yet the region near a flaw or crack may undergo plastic deformation and fracture from locally high stresses, ultimately resulting in premature or catastrophic failure under service conditions. The first documented observation of acoustic emission in

1953 by J. Kaiser [38] was the modern day starting point for its active use. In fact, Kaiser characterized a basic irreversibility phenomenon which bears his name. In the Kaiser effect (Fig 6) when a material is stressed to a given level and the stress removed, upon reloading there is an absence of detectable emission at a fixed sensitivity level until previously applied stress level has exceeded. Since Kaiser's time, advances in both materials science and electronic technology have contributed in bringing acoustic emission to the forefront of new NDT methods.

2.6.1 AE vs Other NDT techniques

The most important reason why the method is now being actively used for testing structures is that it is essentially non localised; it is not necessary for the receiving transducer to be particularly near the source of the emissions or the area which is under test. For example a critical node in an offshore structure could be tested in service by as few as 12 transducers [23] while ultrasonic methods would need about a thousand sensors. It is very easy to scan a large structure using acoustic emission probes placed at 1-10 m intervals on the surface of a structure. This ability to examine a large area of material is in direct contrast to alternative methods of non destructive examination such as ultrasonics or radiography. Ultrasonics in particular requires that a probe must scan over practically every part of the structure to be examined. Another reason why acoustic emission is a particularly attractive NDT tool stems from its value for the continuous in-service monitoring of structures [24].

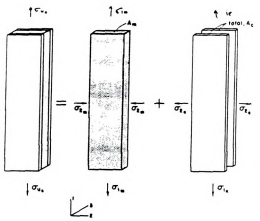

FIG.5. Isostrain model for uniaxial tensile deformation of clad sheet material.

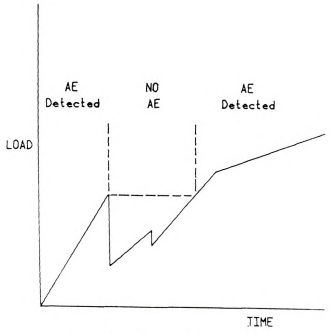

FIG.6. Kaiser effect

This is particularly important in offshore applications where other methods of inspection, which usually requires divers, cannot be used in adverse weather conditions, while acoustic emission monitors will operate 24 hours each day, even in the worst storms when safety monitoring is particularly important. Strain gauges also have a 24 hours a day capability, but require placement very close to a suspected defect. Acoustic emission techniques can detect and evaluate structural significance of flaws (which may be inaccessible to the traditional NDT techniques), thereby , it can give early warning of impending failure. AE is an extremely sensitive test method. To have some ideas of its sensitivity, relative to the more familiar NDT methods, the minimum detectable crack size for ultrasonics , radiography and eddy-current techniques is about 2.54×10^{-3}cm; for strain gauges, about 2.54×10^{-6}cm; and for AE , about 2.54×10^{-12}cm [29]. Thus, the dynamic range of sensitivity to events that can be detected by most basic commercial available AE system extends from gross events that produce audible signals to microevents such as dislocation movements.

2.6.2 Priciples of Acoustic emission

Acoustic emissions (AE), from a composite material are transient elastic waves generated by rapid release of energy within the material as a result of matrix crazing, initiation and propagation of cracks, fretting (or rubbing) at previously damaged area, debonding etc. The energy released propagates through the material as stress waves and is picked up by transducers that are mounted on the surface of the material. The output of the transducers is amplified through a high

gain, low noise preamplifier, filtered to remove any extraneous low frequency noise, conditioned (in a wide variety of ways) and displayed. A typical acoustic emission signal associated with energy released by any of sources mentioned above is shown in Fig 7 [26]. This is called an AE event. The most common ways these signals have been processed in past are:

(a) Counting

The number of times the signal amplitude exceeds a preset threshold during an experiment is called the acoustic emission count (ring down count). This parameter or its time derivative constitutes the commonest method of displaying an acoustic emission result. A lesser used technique is to count the number of acoustic emission events. The number of ringdown counts for an event detected by a transducer is [27]

$$N = \frac{V_r}{\beta} \ln \frac{V_0}{V_t}$$

Where V_r is the resonant frequency of the transducer, β the logarithmic decrement, V_0 the initial voltage, and V_t the threshold voltage. The limitation of such a technique is that the results are strongly influenced by the geometry of the specimen, the properties of the detector and its bonding to the specimen.

(b) Energy analysis

Acoustic-emission energy is generally assumed to be proportional to the integral of the square of the transducer output. The commonly

measured root mean square (RMS) voltage is closely related to the energy rate (ie. acoustic-emission 'power'). The advantage of using the RMS transducer voltage or power measurement is that it gives continuous measurement of a parameter of the emission which can be standardized and used for comparative experiments. It must be emphasized, however, that extreme precautions have to be taken if this is to be related to some source property.

(c) Amplitude analysis

In this technique, which Ono [28] has recently reviewed, the amplitude of the voltage signals from a piezo-electric transducer are plotted as distributions and then compared. It has commonly been found that the number of signals exceeding a specific level is given by

$$N(a) = (V/V_0)^{-b}$$

Where V is the amplitude of a transducer voltage, V_0 the lowest detectable amplitude, and b is the distribution characteristic. The b-value has been used to characterize emission from different processes. Typically b is in the range 0.2-0.4; small b-values being indicative of a high proportion of energetic relaxation events. There is, however, no fundamental importance in a precise b-value measured in an experiment, but it can serve empirically to characterize different forms of emission.

(d) Frequency analysis

Frequency analysis can yield information about source rise time and fracture type [30]. However unless extreme precautions are taken the analysis is limited to the observation of changes in the frequency spectrum which, can be correlated with different types of deformation processes. The most commonly employed method of extracting frequency information from emission is a digital one in which the emission waveform after amplification is passed into a transient recorder to digitize the waveform for subsequent access by a small computer. Standard Fourier transform routines then permit frequency analysis. This digital approach requires a digitization frequency and so broad-band width systems are currently limited by existing technology to about 50 MHZ because the maximum digitization rate is 100 MHZ. However almost all frequency analysis has been done with narrower band width systems, with an upper frequency limit of about 5 MHZ. Graham and Alers [31] applied frequency analysis to emissions produced during deformation and fracture of a pressure vessel steel. They found that in their frequency range (up to 2 MHZ) two distinct types of spectra were observed; One which was associated with plastic flow and other with crack extension. Speake and Curtis [20] using a limited band width detection system, but using constant-geometry specimens and varying only the fracture process, were able to show that changes in frequency content of the detected emissions could be correlated with different failure processes in carbon-fibre reinforced plastics. This significant result showed that different types of failure processes could be identified by frequency analysis as long as other variable were controlled.

2.6.3 Acoustic emission technique instrumentation

A block digram of 3000 PAC Acoustic emission technique system is shown in Fig 8. The physical appearance of the system will be shown in experimental procedure chapter.

Acoustic emission signals are detected by transducers attached to the specimen. Detected emission stress waves are amplified by a preamplifier. The preamplified signals are received via cables at the signal processing unit, where the signals are filtered to reduce the effects of signals from the grips and vibration or shocks from nearby machines. After filtering, the signals are further amplified and a single pulse is formed indicating time of arrival of the emission signal.

The pulses generated by sensors are selected for input to the time analysis logic which generates the time of arrival differences or ΔT used in flaw triangulation. The pulses from signal conditioners are also used to derive emission rate, total emission and energy. In the 3000-3004 PAC acoustic emission system, the emission rate can be expressed in either emissions per unit time or emissions per unit load, because of the added feature, external parameter input, capable of accepting an external parameter voltage 0-1 Volt (D C) level (or 0-10 Volt). AE data is stored in a computer, which is programmed to collect and process AE data.

2.6.4 Theoretical calculations for flaw location

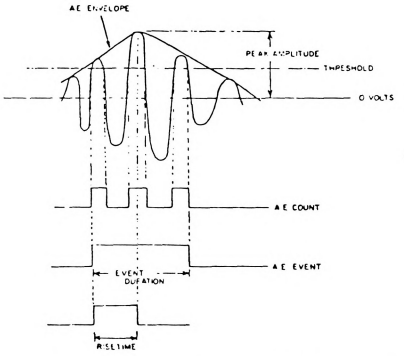

FIG.7. AE burst and associated definitions [26]

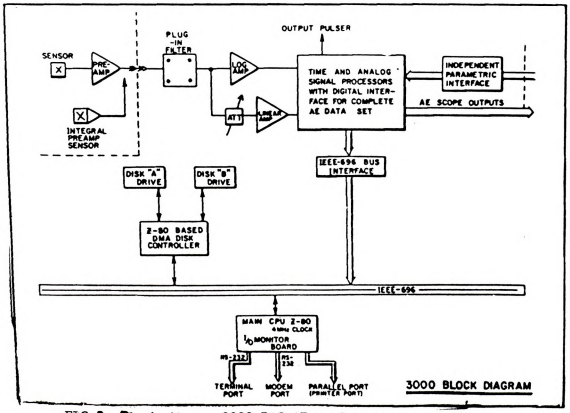

FIG.8. Block digram, 3000-PAC AE analysis system [26]

In the linear flaw locations, two transducers are positioned on the sample as shown in Fig 9. The signals from the source arrives at the two transducer with different arrival times. The distance X, from the source to mid point between the transducers is given by

$$X = l\,(Ta-Tb)/2$$

where Ta is the arrival time at transducer a, Tb is the time of arrival at transducer b and l is a constant [32] describing the speed of the wave and its attenuation in the material. It is determined experimentally by a caliberation procedure. The parameter (Ta-Tb) is determined electronically using a clock.

Location for an AE source in a three dimensional body requires (a) measurement of arrival times of AE wave at four sensors; (b) positions of four sensor and; (c) an appropriate speed of sound for the test body.

The theory, for calculation of flaw location (from the above data) follows. The theory assumes that the operating AE source propagates at a contant velocity, spherically expanding impulsive mechnanical disturbances into an infinite medium. Let M,N,U,W be the labels given to the four sensors in an array. These sysmbols also represent vectors of position for the four sensors. Tm,Tn,Tu,Tw identify arrival times of the AE wave at each of the four sensors. The M sensor is assumed to be the first sensor struck in this discussion.

The relations

$$\Delta N = (Tn-Tm)\times C$$

$$\Delta U = (Tu-Tm)\times C$$

$$\Delta W = (Tw-Tm)\times C$$

express the distance the acoustic wave travels to reach each of the last three sensors struck, in addition to the distance it traveled

to strike the first sensor, M. In these expressions, C is the appropriate velocity of sound.

The total distance, D the acoustic wave traveled to reach each transducer can be expressed by the matrix equations

$$|M - P| = D$$

$$|N - P| = D$$

$$|U - P| = D$$

$$|W - P| = D$$

where

$|\ |$ = Vector length and

P = Vector of position for the source point, and the unknown quantity to be calculated.

Unknown quantities P and D can be determined from the above equation. Detailed solution was given by Tatro and Brown [33].

2.6.5 Factors affecting AE reponse

There is a great variety of acoustic emission produced by materials. Some material produce acoustic emission copiously when stressed, while others are quite by comparison. The AE from a smooth tension specimen with a crack differs markedly from that observed from tension specimen without a crack. Fig 10 shows continuous acoustic emission from an unflawed mild steel specimen [34] during tension test. A peak in AE can be seen at the yield stress of material. The continuous acoustic emission is highly strain rate sensitive. Materials containing fatigue cracks yielded primarily burst type AE as the plastic zone formed at the fatigue crack tip. Thickness effects also influence the amplitue of the burst type emissions from specimen

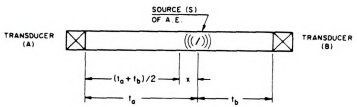

FIG.9. Linear localization using two AE transducers.

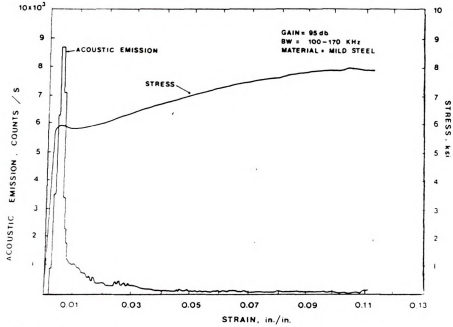

FIG.10. Acoustic emission and stress as a function of strain for a mild steel tension specimen.

containing sharp cracks. Higher amplitude acoustic emission signals were obtained from the thicker specimen. The reason may be the existance of higher triaxial stresses in the vicinity of the crack front in the thicker specimen. Another factor that influences the amplitude of acoustic emission is basic crystalline structure. Materials such as tin, uranium and beryllium usually result in higher amplitude signals in comparison to fcc materials which are more isotropic. Fig. 11 shows the result of a of typical tension test with organic fiber composites. This figure shows the band within which the sum of AE versus the load fell for 14 specimens, [35] the actual curves for two of these non flawed specimen and the actual curves for two flawed specimens. It has been determined [36] that acoustic emission, n, as a function of stress intensity, K could be expressed as

$$N = AK^m$$

where N = Total cumulative acoustic emission,

A = Proportionality constant

K = Stress intensity = $\alpha\sigma\sqrt{a}$

m = Empirically derived exponent

α = Geometry function (sample)

σ = Stress at proof load

a = Initial size of defect

2.7 X radiography and ultrasonic NDT

In the past, both X radiography and ultrasonic C-scan have been used in the evaluation of nonmetallic composite materials [41,42]. The X radiography technique utilizes an x-ray opaque compound,

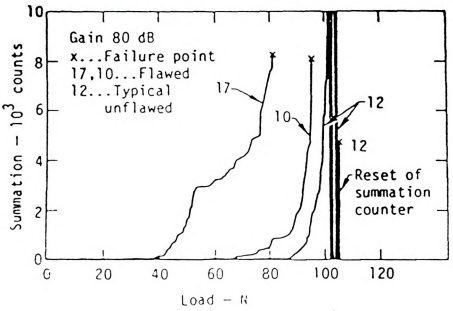

FIG.11. AE of flawed and unflawed organic fiber-epoxy strand specimens.

tetrabromethane (or zinc iodide), which is very effective for use with porous materials. Since the compound can penetrate porous materials, defects appear as high film density area on the radiographic film and can be readily detected.

Ultrasonic imaging technique, which obtain images by the attenuation properties of material, is also a tool for detecting the defect at the interface of composite materials. The range resolution depends on operating frequency [43]. Ultrasonic imaging technique provides a dual display of B and C scan simultaneously and thus allows a rapid identification of the defects at the interface.

III. EXPERIMENTAL PROCEDURES AND TECHNIQUES

3.1 Fabrication of Cu-Ni composite

15.24 cm × 15.24 cm × .318 cm square plates of Ni 200 (Ni=99.5 pct,C=0.03pct,Mn=.22pct,Fe=0.15pct,Si=0.05,Cu=0.05pct) were procured from International Nickel Company. The square plates were machined into (7.62 cm × 2.18 cm × .32 cm) rectangular pieces. Each of these pieces was rolled to a thickness of 0.33mm. All pieces were annealed at 750^{0}C for 5 minutes. Before annealing the nickel pieces (12.7 cm × 2.13 cm × .33 cm) were covered with 3 layers of copper foil (.005 cm) to minimize oxidation. After annealing the nickel plates were heated in the following pickling solution to loosen the scale (oxidized layer) at 74^{0}C for 1 hour and 30 minutes [39]

Water	316 ml
Hydrochloric acid	158 ml
Cupric chloride	10 gm

The nickel pieces were then rinsed in hot water and dipped in another solution (composition below) to remove the scale.

Water	71.69 ml
Sulphuric acid	98.68 ml
Nitric acid	161.32 ml
Hydrochloric acid	5.0 ml

After pickling, the nickel pieces were polished on abrasive grit paper to produce a shiny surface. At this point, the nickel pieces

were ready for electroplating. For plating copper on nickel, a two step method was used. Cyanide bath plating was first performed, followed by acid plating. Acid plating does not produce a good bond between copper and nickel, but the process does not limit the thickness of copper deposited. This is in direct contrast to the cyanide plating process where the bonding is good, but a limit exists on the thickness of the copper plated (1-2 mil). For making Cu-Ni composites good bonding and thicker deposits were needed, hence a combination of two plating processes was chosen.

(a) Cyanide copper plating

This plating technique was used to put a strike of cyanide copper on the nickel plate. Copper so deposited has good bonding,because in this technique copper gets deposited only by ion discharge on cathode (nickel).

Bath composition

Copper(cuprous) cyanide	3.0 oz/lit
Sodium cyanide	4.5 oz/lit
Na-thiosulphate(hypo)	2.0 oz/lit

Current density used was 15.06 mamp/sq cm

Temperature of bath was kept at 34-36^{0} C

Cyanide copper plating on nickel was carried on for 45 minutes. After this plating the nickel piece (with a strike of copper) was

washed in water thoroughly (to wash away cyanide) and then dried, to prepare for the next plating process.

(b) Acid copper plating

This plating process was used to plate copper on the nickel to the full thickness (equal to nickel plate thickness). This plating produced copper plating with few coarse grains (compared to cyanide plating). The temperature of the bath was controlled by switching the heater ON and OFF manually (at 29^{0}C) or temperature was controlled by temperature controller (fish tank temperature controller). The bath was stirred magnetically through-out plating to avoid polarization.

Bath composition

Cupric sulphate	200 gm/lit
Sulphuric acid	50 gm/lit

Phenol sulphuric acid (equal volume of Phenol and sulphuric acid heated at 100^{0}C for 1 hr) was used as smoothing agent (1gm/lit).

Current density used was 26.35 mamp/sq cm

Temperature of bath maintained was 29-30^{0}C

Two kinds of Cu-Ni composites were made, symmetric (Cu-Ni-Cu) and asymmetric(Cu-Ni) composites. While making asymmetric composite, one side of the nickel plate was masked with lacquer before copper plating. The lacquer layer was removed with acetone after the plating.

3.2 Artificial defects

Some symmetric composite specimens were made with voids of known dimensions at the interface (on one side of the symmetric composite). Defects were introduced by putting scotch tape (0.02 mm thick) of different sizes (rectangular) on the nickel plate, before copper plating. Those pieces of scotch tape acted like discontinuities at the interface. A digramatic sketch of some specimens showing defect size and location, will be shown with the results and discussions.

3.3 Tensile test.

Two types of tensile specimens were made. One was ASTM B557 subsize (rectangular) test specimen. The other type was made with all the dimensions reduced by one half. From each composite plate either two big tensile specimens were made or 6 small tensile specimens. The shape of the big and small specimens are shown in Fig 12. The dimensions of the big and small follow (with reference to fig 12):

	Big specimen	Small specimen
G	1.000±.003	0.5±.003
W	0.250±.002	0.125±.002
T	thickness	thickness
R	.25	.25
L	2.0	1.0
A	1.25	.625
B	1.25	.625
C	.375	.188

All dimensions are in inches.

Small grips were used for pulling both tensile specimens. First one annealed and one unannealed big specimens were pulled in Instron

machine. These specimens showed the phenomenon of cupping so we had to work with symmetric specimens later on. During all the tension tests, acoustic emissions from the tensile specimens were collected, using 3000-3004 PAC acoustic emission machine.

3.4 Acoustic emission testing

The experimental setup for Instron cum acoustic emission testing is shown in Fig 13. The position of transducers on the surface of the specimen (during tension test) is shown in Fig 14. Acoustic emission was detected by coupling a piezoelectric(PZT) transducers directly to the specimen with silicon grease. The signals from the sensors were preamplified and filtered before being sent to the AE machine. System gains of 3,15,21 db and band pass of 100-300 KHZ were used. Of the four transducers, two were used as safeguard (to discard the AE signals from grips or machine). All AE data was collected by the computer (attached to AE machine). Data (plots) could be monitored during data collection or stored for future processing. Software RT/DAS and RT/DAQ were used for AE data acquisition. Super Plot software was used to produce hard copies of AE parameter plots.

For linear location of defects the sensors had to be calibrated using an average value of delta-t (location distance) obtained with a pulser. This was done by placing a pulser next to one of the two sensors. Readings were taken and the average delta-t was stored in memory. This delta-t value was then used to calculate the linear location of the AE source on the specimen using the algorithm described previously.

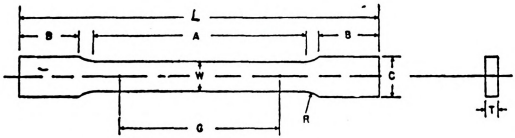

FIG.12. Tension test specimen

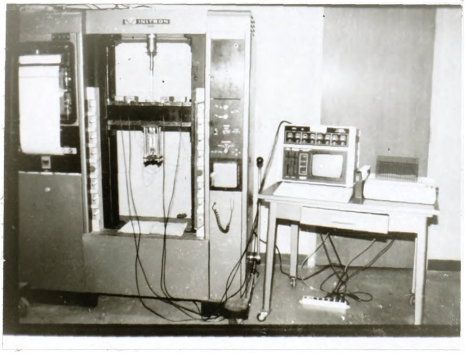

FIG.13. Experimental setup

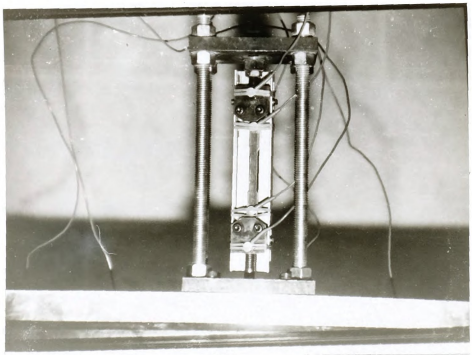

FIG.14. Figure showing the positions of transducers on the tensile specimen.

3.5 Electron microprobe

For analysing the composition profile at the interface using a microprobe, a transverse section of specimens after tensile tests was mounted on cold setting epoxy resin and polished on 240,320,400,600 emery paper. The final polishing was done on a polishing wheel with microcloth using 0.05 micron alumina. The specimens were etched in 50 pct nitric acid + 50 pct acetic acid etchant for 25 seconds, to get rid of the smeared film of metals. Microprobe voltage of 25 kv was used. Two spectrometers were used simultaneously to handle Cu and Ni concentrations separately. From the composition profile (of the interface) obtained from the microprobe plotter, the length of the diffusion zone was calculated.

3.6 Scanning electron microscopy

The specimen preparation was essentially the same as that used for the electron microprobe, the only difference, being that in this case the specimens were etched for 10 seconds. A Hitachi 5-415 scanning electron microscope was used for studying delamination and cracks at the interface. A polaroid camera attachment was used to take micrographs at the specimen interface.

3.7 Ultrasonic test and Radiography

An ultrasonic machine (pulse echo) at Oldsmobile was used to confirm the presence of artificial defects at the interface qualitatively. The transducer frequency was 15 MHZ and amplification

was 23 db. The resolution of the signals from the transducer was increased by the use of polystyrene between the transducer and metal composite. Pictures of the A-scan from some of the samples (with defects) were taken, although all of them were scanned for confirmation of presence of defects. Ultrasonic imaging of the composite was tried in Dr. Ho's laboratory, but defects could not be resolved because of the low frequency transducer, used in his system.

A X-ray machine in the Bio-mechanics department was used for taking X-radiographs of specimens (with defects) to confirm the presence of defects at the interface. The voltage was 66 kv and exposure time was varied from 1 to 3 seconds. Only some of the defects could be resolved. Resolution of defects was not good.

IV. RESULTS AND DISCUSSION

For the present study, asymmetric (Cu-Ni) composite were considered. They were studied for their mechanical and acoustic response. An extra feature, cupping during tension was analysed theoretically for the asymmmetric composite (one layer of either metal). An expression for predicting the radius of curvature during tension, for an unbonded composite was derived and compared to the result obtained from the bonded asymmetric composite. The fracture surface of annealed and unannealed Cu-Ni composites was inspected under a scanning electron microscope. The SEM micrographs and the acoustic emission response is presented followed by the theoretical illustration of cupping.

For the second half of the study symmetric composite (Cu-Ni-Cu) were made. Their mechanical and acoustic response was studied with respect to varying thickness, heat treatment and strain rate. The composition profile of the interface with different diffusion times at particular temperature is presented after the SEM micrographs of the fracture surface. The Kaiser effect was proved for the symmetric Cu-Ni-Cu composite. Lastly the role of artificial voids (at the interface) in the mechanical response of symmetric Cu-Ni-Cu composites is illustrated using the acoustic emission parameters.

(a) Pure copper and pure nickel

time

200.

AE c

ten

exp

dat

eff

cor

te

po

Fig. 15 and Fig. 16 show the joint stress-strain and AE counts-time plot for the pure Cu (annealed at 750^{0}C for 5 min) and pure Ni 200. The data for pure metals were obtained to see the correlation of AE characteristics with tensile properties (individually). Ultimate tensile strength for pure Cu and pure Ni 200 was obtained experimentally by using small size specimens. Table 2 shows the UTS data obtained. The variation observed, depends on the localised notch effect (created during machining). Two peaks of AE counts are consistant with the AE data Pisarenko et-at [43] obtained during tension test of the Amg-6 alloy. The first peak represents the yield point.

TABLE 2 Tensile properties of Cu and Ni specimens used.

Metal	Reading	UTS(kg/mm^2)	Average UTS(kg/mm^2)
Copper	1	21.54	
(annealed	2	21.23	
at 750 C	3	20.48	21.69
for 5	4	23.5	
minutes			
Nickel	1	48.81	
(annealed	2	50.47	50.25
at 750 for	3	51.76	
5 minutes			

(b) Asymmetric Cu-Ni composite

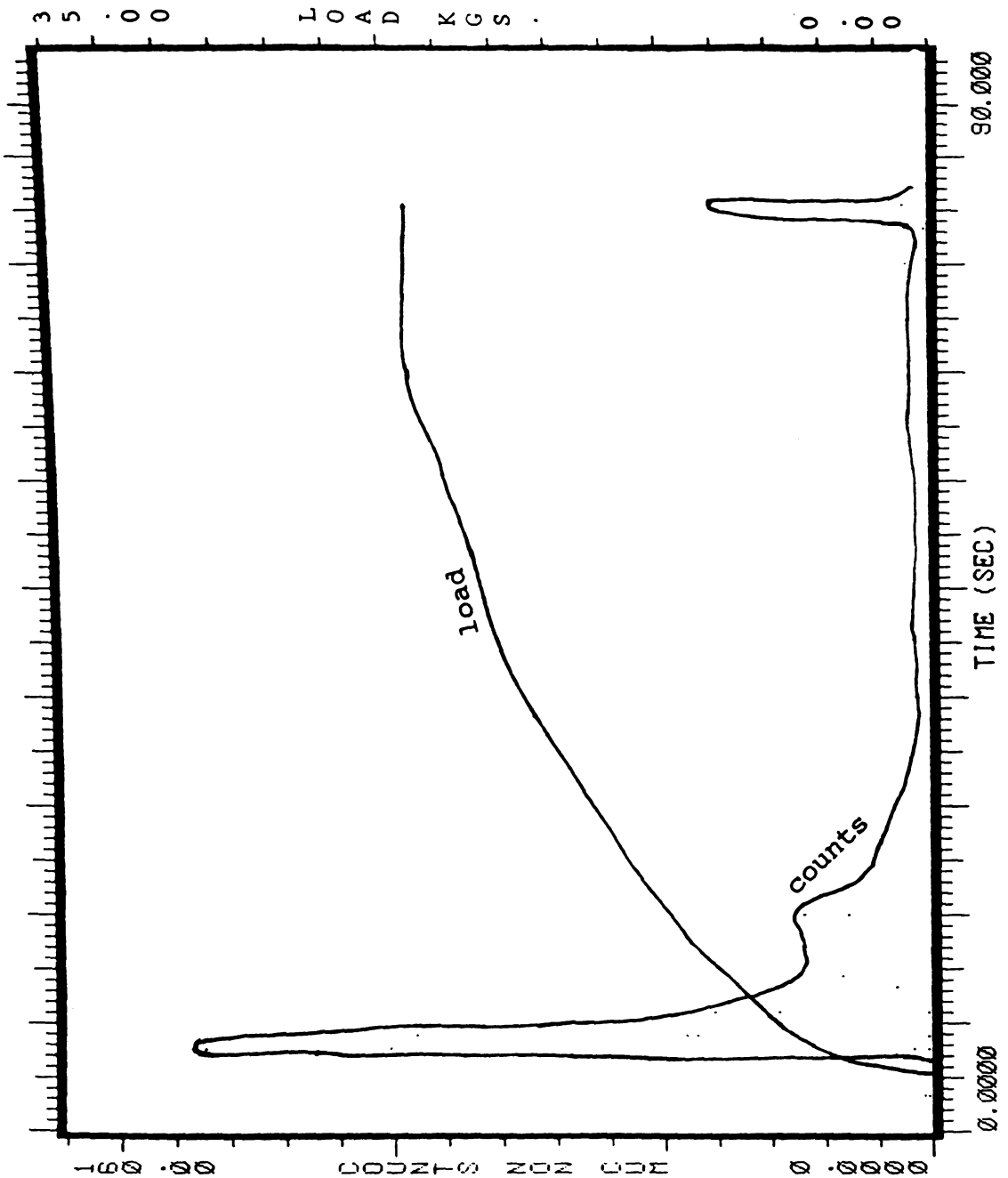

FIG.15. Acoustic emission and stress as a function of time of pulling for a copper tension specimen.

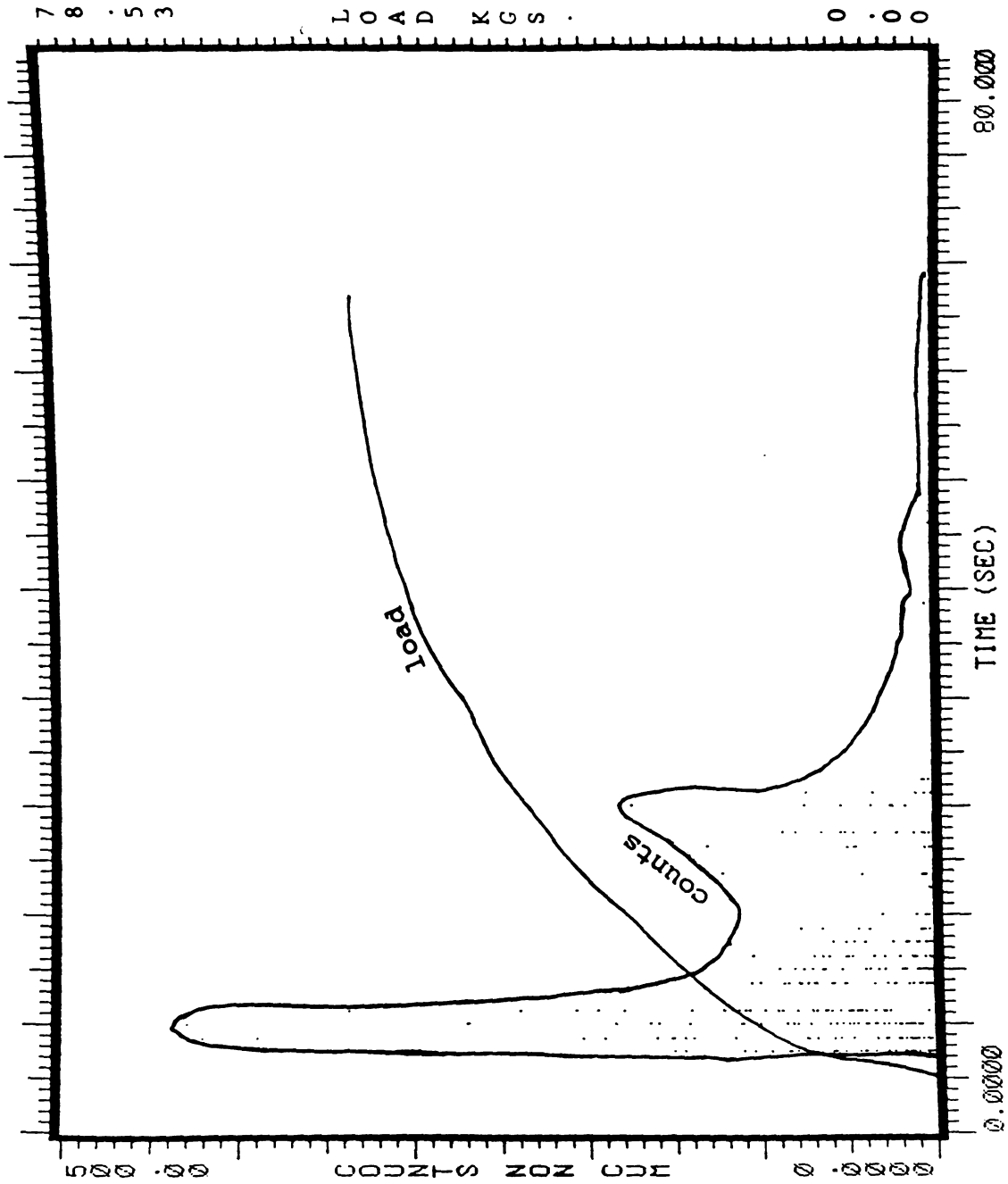

FIG.16. Acoustic emission and stress as a function of time of pulling for a nickel tension specimen.

O

minute

asymme

The s

strong

could

annea

of a

inter

conc

unan

not

dela

copy

and

dep

dep

and

cop

du

to

of

f

c

c

One asymmetric Cu-Ni composite was annealed at 750°C for 5 minutes and was tested in tension. Under the same conditions one asymmetric plated (unannealed) Cu-Ni composite was tested in tension. The stress strain curve showed that the unannealed composite was stronger (48.25 kg/mm^2) than the annealed (39.80 kg/mm^2) one. It could be explained by the SEM micrograph of transverse sections of annealed and unannealed specimens (Figs 17 - 20). The microstructure of annealed specimens show the existance of many voids at the interface. Those voids coalesced to form a crack and led to stress concentration and premature failure. The SEM microsturctures of unannealed specimens show a strong bonding at the interface, it does not show delamination where as in the annealed specimen some delamination is quite evident (in Fig.18). Some severe cracks, on the copper side, can be seen in the microstructure of both the annealed and unannealed specimens. These cracks are due to the dendritic deposition of copper on the outer side of copper layer. The dendritic deposition occured due to insufficient stirring of the plating bath and poor temperature control. That led to low strength of the outer copper producing cracks.

The cup produced in the asymmetric Cu-Ni tension specimen is due to the difference in Poisson ratios of Copper and Nickel, i.e due to the different transverse strain produced. Theoretically the radius of cupping can be derived by using complicated boundary conditions and finite element methods. The expression for radius of cupping of cupping (under tension) for the unbonded Cu-Ni laminate (1 layer each) can be derived as follows:

In Fig.21 and Fig.22 layer 1 represents Copper layer and layer 2 represents Nickel. In equillibrium

FIG.17. SEM micrograph of transverse section of unannealed Cu-Ni composite tensile specimen (below fracture surface).

FIG.18. SEM micrograph of same position(above) only interface magnified.

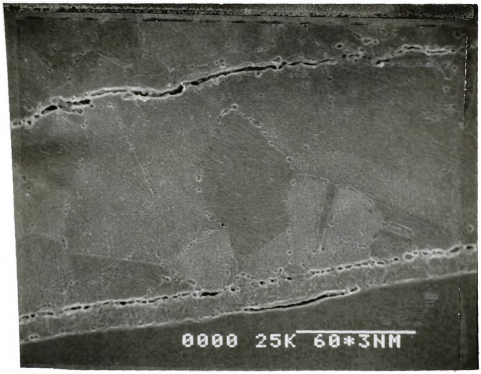

FIG. 19. SEM micrograph of an Cu-Ni composite tensile specimen annealed at 750 C for 5 minutes (just below fracture surface).

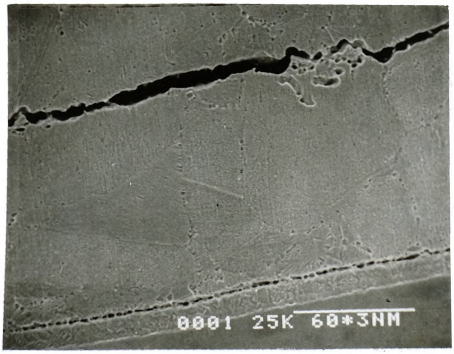

FIG.20. SEM micrograph same as above,magnified.

FIG
pla

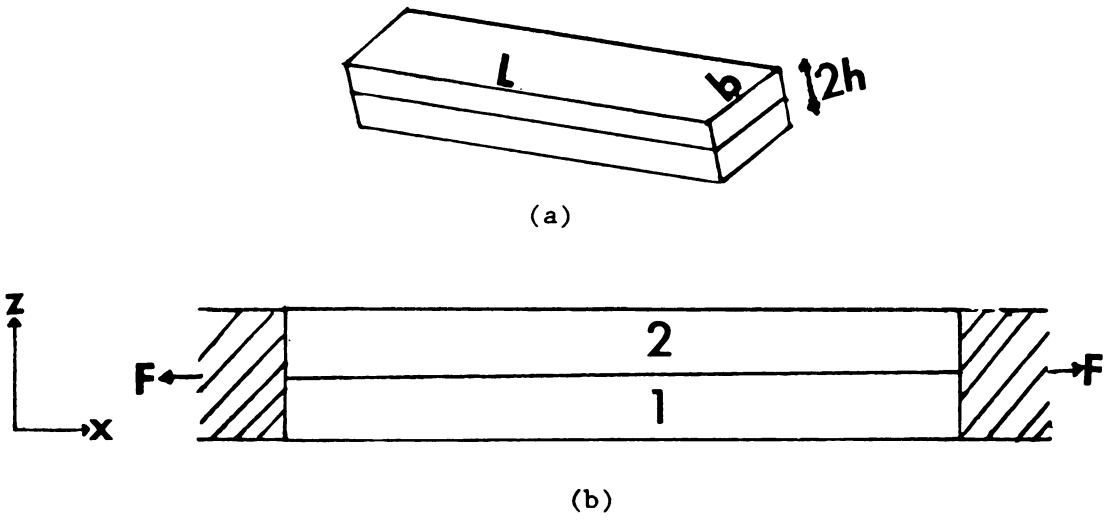

FIG.21. Assymetric Cu-Ni composite,(a) shows a composite plate (b) shows the loading conditions in tension.

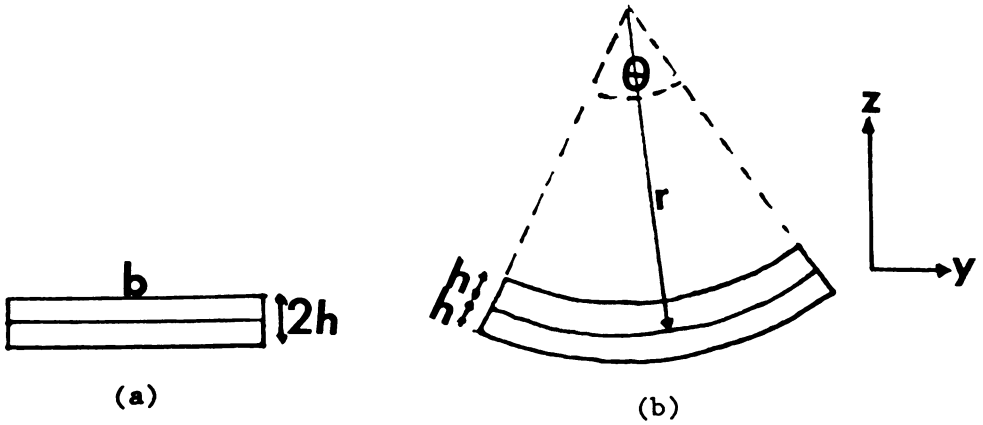

FIG.22. (a) Cross section of Cu-Ni composite plate (b) shows the curved cross section with radius of curvature.

F =

where

A_1 and A_2

case A_1 =

ϵ_{1x}

By g

ϵ_{1y}

ϵ_{2y}

Thr

(i)

ϵ_{1}

Ho

F

$$F = \sigma_1 A_1 + \sigma_2 A_2 \qquad \ldots\ldots\ (1)$$

where σ_1 and σ_2 are stresses on the copper and Nickel layers. A_1 and A_2 are cross sectional area for Cu and Ni layers. (In our case $A_1 = A_2$) . By compatibility

$$\epsilon_{1_x} = \epsilon_{2_x} \qquad \ldots\ldots\ (2)$$

By geometry

$$\epsilon_{1_y} = \frac{(r-h/2)\theta - b}{b}$$

$$\epsilon_{2_y} = \frac{(r+h/2)\theta - b}{b} \qquad \ldots\ldots\ (3)$$

Three cases can be considered (for tensile deformation)

(i) Both metals in the elastic range.

$$\epsilon_{1_x} = \epsilon_{2_x}$$

Hook's law ; $\frac{\sigma_1}{E_1} = \frac{\sigma_2}{E_2}$ and $A = A_1 = A_2$

$$\sigma_1 = \frac{FE_1}{A(E_1+E_2)} \quad ; \quad \sigma_2 = \frac{FE_2}{A(E_1+E_2)}$$

$$\epsilon_1 = -\frac{\nu_1}{E_1}\sigma_1 = -\frac{\nu_1 F}{A(E_1+E_2)} \qquad \ldots\ldots(4)$$

$$\epsilon_1 = -\frac{\nu_2}{E_2}\sigma_2 = -\frac{\nu_2 F}{A(E_1+E_2)} \qquad \ldots\ldots(5)$$

From geometry and equation 4 and 5 :

$$r = \frac{h}{2}\left\{\frac{2A(E_1+E_2) - (\nu_1+\nu_2)F}{(\nu_1-\nu_2)F}\right\}$$

where r = radius of cupping (shown in the figures)

(ii)

ϵ_2^t

from

ϵ_{1_X}

ϵ_{1_X}

ϵ_{2_X}

σ_1

Fr

F

S

(loadi

determi

T

I

deter

(ii) When layer 1 elastic(nickel) and layer 2 plastic(copper):

$$\epsilon^t_{2x} = \epsilon^e_{1x} + \epsilon^p_{2x} \quad ; \quad \epsilon^p_{2x} = \left(\frac{\sigma_2}{K_2} \right)^{1/n_2}$$

from equation 2

$$\epsilon_{1x} = \epsilon_{2x}$$

$$\epsilon_{1x} = \frac{\sigma_1}{E_1}$$

$$\epsilon_{2x} = \frac{\sigma_2}{E_2} + \left(\frac{\sigma_2}{K_2} \right)^{1/n_2}$$

$$\sigma_1 = E_1 \left\{ \frac{\sigma_2}{E_2} + \left(\frac{\sigma_2}{K_2} \right)^{1/n_2} \right\}$$

From equation (1)

$$F = A \left\{ E_1 \left(\frac{\sigma_2}{E_2} + \left(\frac{\sigma_2}{K_2} \right)^{1/n_2} \right) + \sigma_2 \right\} \qquad \ldots\ldots(6)$$

Since F, A, E_1, E_2, K_2, n_2 are can be found at a certain F (loading) range. Solving equation (4) the value of σ_2 can be determined Also , $F = (\sigma_1 + \sigma_2)A$; or $\sigma_1 = (F - \sigma_2 A)/A$

The value of σ_2 can be determined from above equation.

Now $\epsilon_{1y} = - \frac{\nu_1}{E_1} \sigma_1$

$$\epsilon_{2y} = - \frac{\nu_2}{E_2} \sigma_2 - \frac{1}{2} \left(\frac{\sigma_2}{K_2} \right)^{1/n_2}$$

From the above two equations value of ϵ_{1y} and ϵ_{2y} can be determined.

Now from equation set (3)

(iii) Bot

ϵ_{1_x}

ϵ_{2_x}

ϵ_{1_x}

t

from

follo

it

$$r = \frac{h}{2}\left[\frac{\epsilon_{1y} + \epsilon_{2y} + 2}{\epsilon_{2y} - \epsilon_{1y}}\right]$$

(iii) Both layers are in plastic range

$$\epsilon_{1x} = \frac{\sigma_1}{E_1} + \left(\frac{\sigma_1}{K_1}\right)^{1/n_1}$$

$$\epsilon_{2x} = \frac{\sigma_2}{E_2} + \left(\frac{\sigma_2}{K_2}\right)^{1/n_2}$$

$$\epsilon_{1x} = \epsilon_{2x}$$

$$\text{therefore,} \quad \frac{\sigma_1}{E_1} + \left(\frac{\sigma_1}{K_1}\right)^{1/n_1} = \frac{\sigma_2}{E_2} + \left(\frac{\sigma_2}{K_2}\right)^{1/n_2} \qquad .....(7)$$

$$\text{Also ,} \quad F = (\sigma_1 + \sigma_2)A \qquad .....(8)$$

From equations 7 and 8 value of σ_1 and σ_2 can be determined.

$$\text{Now} \quad \epsilon_{1y} = -\frac{\nu_1}{E_1}\sigma_1 - \frac{1}{2}\left(\frac{\sigma_1}{K_1}\right)^{1/n_1}$$

$$\epsilon_{2y} = -\frac{\nu_2}{E_2}\sigma_2 - \frac{1}{2}\left(\frac{\sigma_2}{K_2}\right)^{1/n_2}$$

From above two equations ϵ_{1y} and ϵ_{2y} can be determined. Now from equation set (3), the radius of cupping r can be given as following:

$$r = \frac{h}{2}\left[\frac{\epsilon_{1y} + \epsilon_{2y} + 2}{\epsilon_{2y} - \epsilon_{1y}}\right]$$

The above expression has to be modified to a great extent to make it applicable to the bonded laminates. The result obtained

theoretic

was fou

were not

4.3

Fi

for the

Acousti

applie

specim

total

compar

shows

for t

speci

acous

voids

orga

plas

plot

ever

voi

for

min

sp

theoretically (for asymmetric specimens) from the expression for 'r' was found to be 200 times more than the experimental; i.e if they were not bonded the radius of cupping would have been much smaller.

4.3 Symmetric Cu-Ni composite

Fig.23 shows the joint AE counts-time and amplitude-time curve for the tension test of unannealed symmetric (Cu-Ni-Cu) composite. Acoustic emission was not emitted until a higher load of 35 kg was applied. Fig. 24 shows the AE counts vs tensile load for the same specimen. This curve is very similar to the stress-strain curve. The total number of AE counts was about 500 which was many fewer when compared to the annealed specimens. Also the delayed acoustic emission shows that the bonding at the interface was good.

Fig.25 shows the joint AE counts-time and amplitude-time curve for tension test of a symmetric composite (same thickness as before) specimen annealed for 35 minutes at 800^{o}C . The early start of acoustic activity was due to the voids present at the interface. Those voids were produced during annealing due to the evaporation of some organic compound at the interface. The AE emissions are due to the plastic deformation of the region near the voids. Fig.26 shows the plot of AE counts vs load for the same specimen. The plot shows that even a small load of 5.5 kgs produced, enough stress, near some of the voids to cause local plastic yielding.

Fig.27 shows the joint AE counts-time and amplitude-time curve for the tension test of a symmetric composite specimen annealed for 60 minutes at 800^{o}C. This specimen seems to be better than the previous specimen (35 minutes annealed). At two place in the AE counts-time

FIG.
tens
(sm

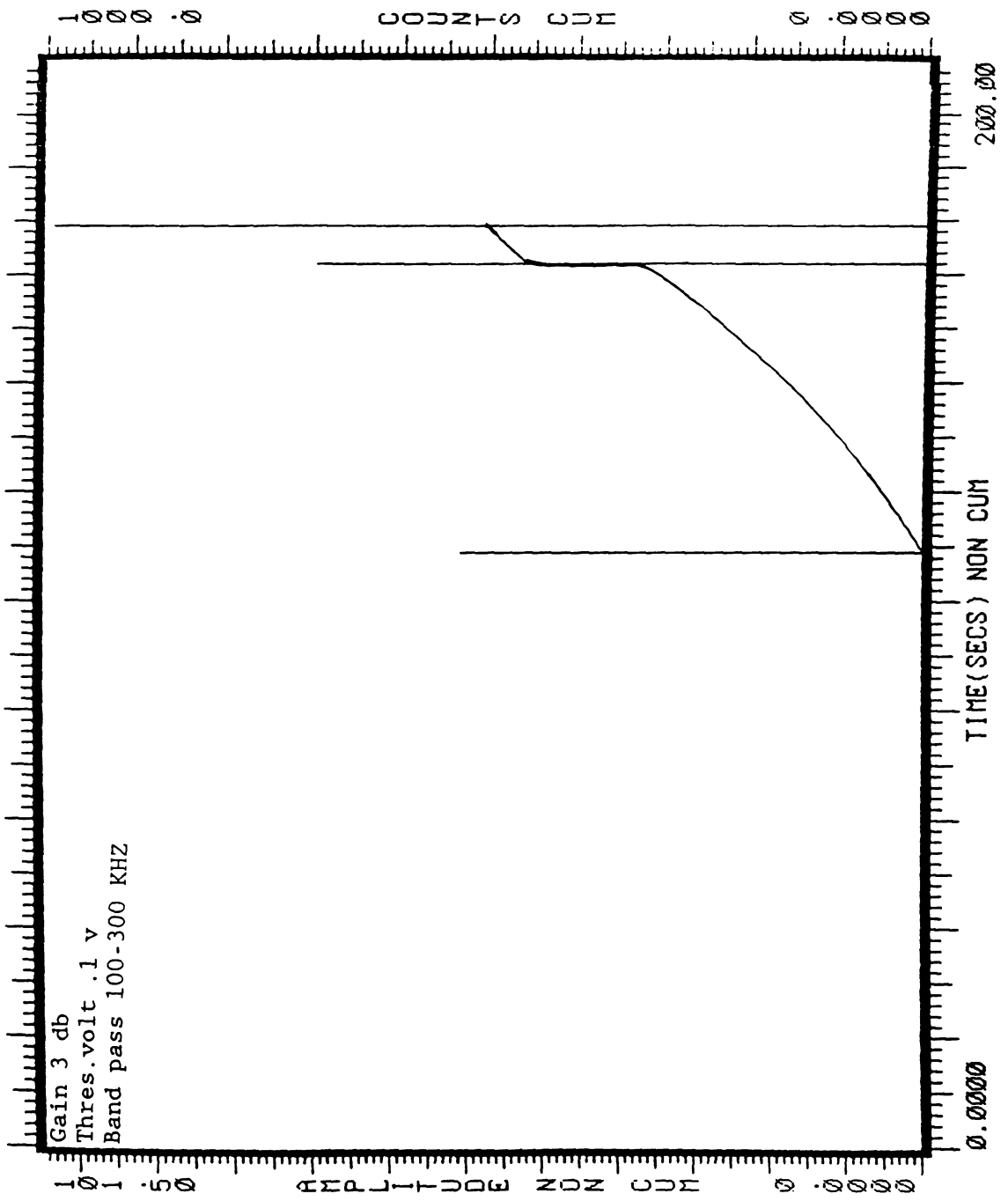

FIG.23. Joint AE counts-time and AE amplitude-time curve for tension test of unannealed symmetric(Cu-Ni-Cu) composite (small tensile specimen).

FIG
sym

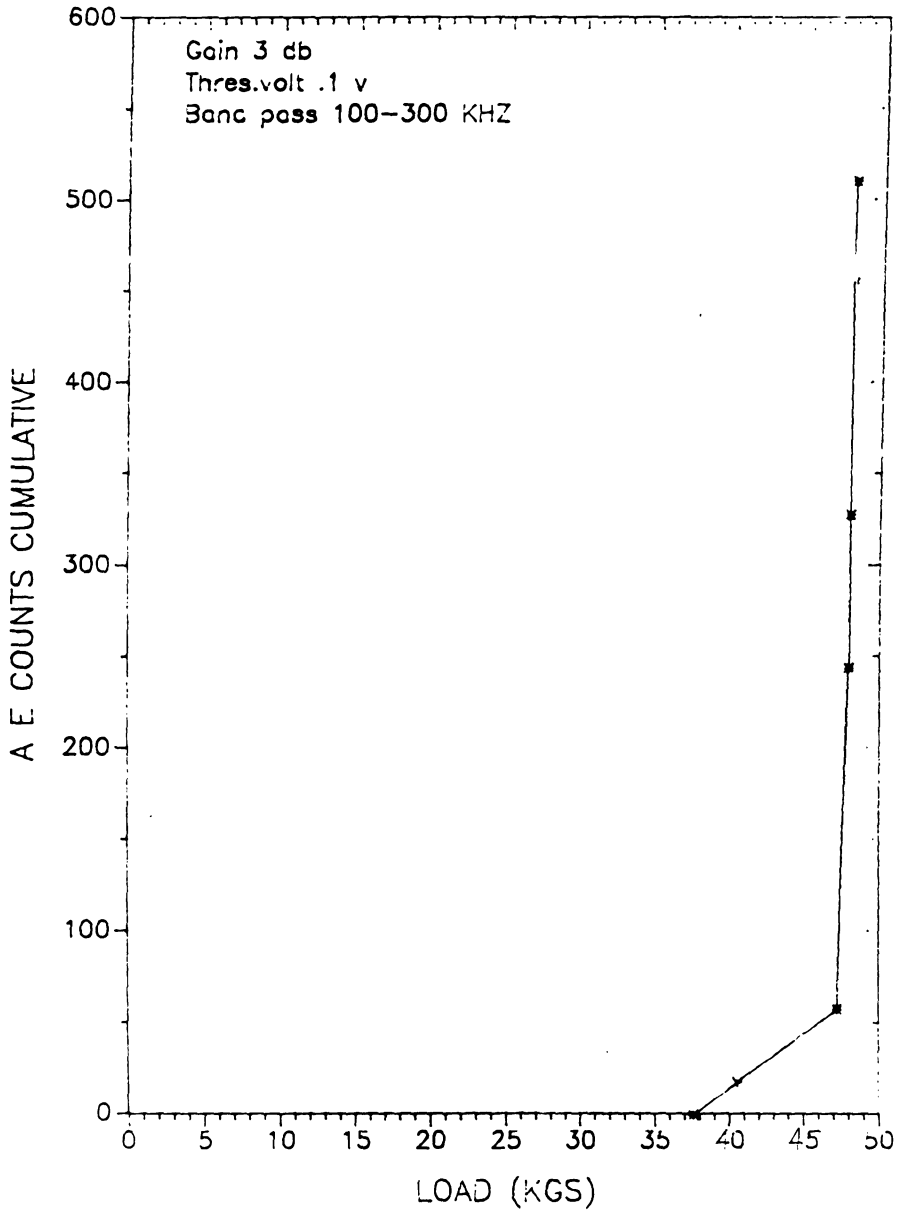

FIG.24.AE counts-load curve for tension test of unannealed symmetric(Cu-Ni-Cu) composite specmen (small).

FI
te

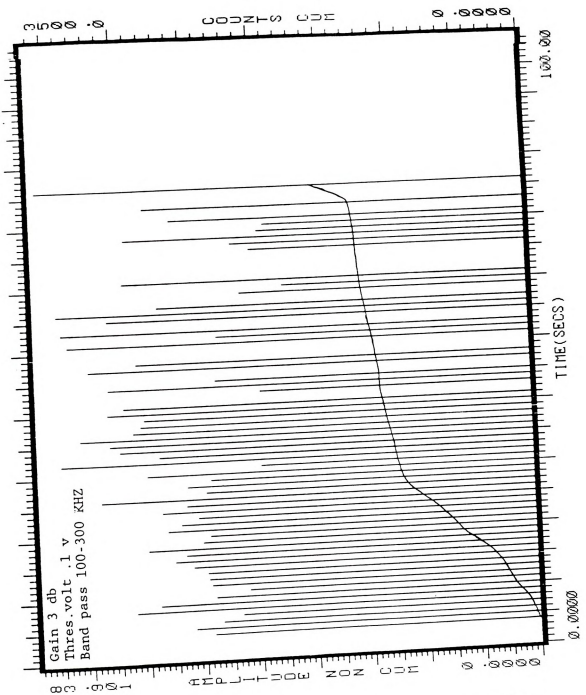

FIG.25. Joint AE counts-time and AE amplitudetime curve for tension test of sysmmetric(Cu-Ni-Cu) composite specimen annealed at 800 ^{0} C for 35 minutes.

200

16

A E COUNTS CUMULATIVE

1

FI

Cu

m

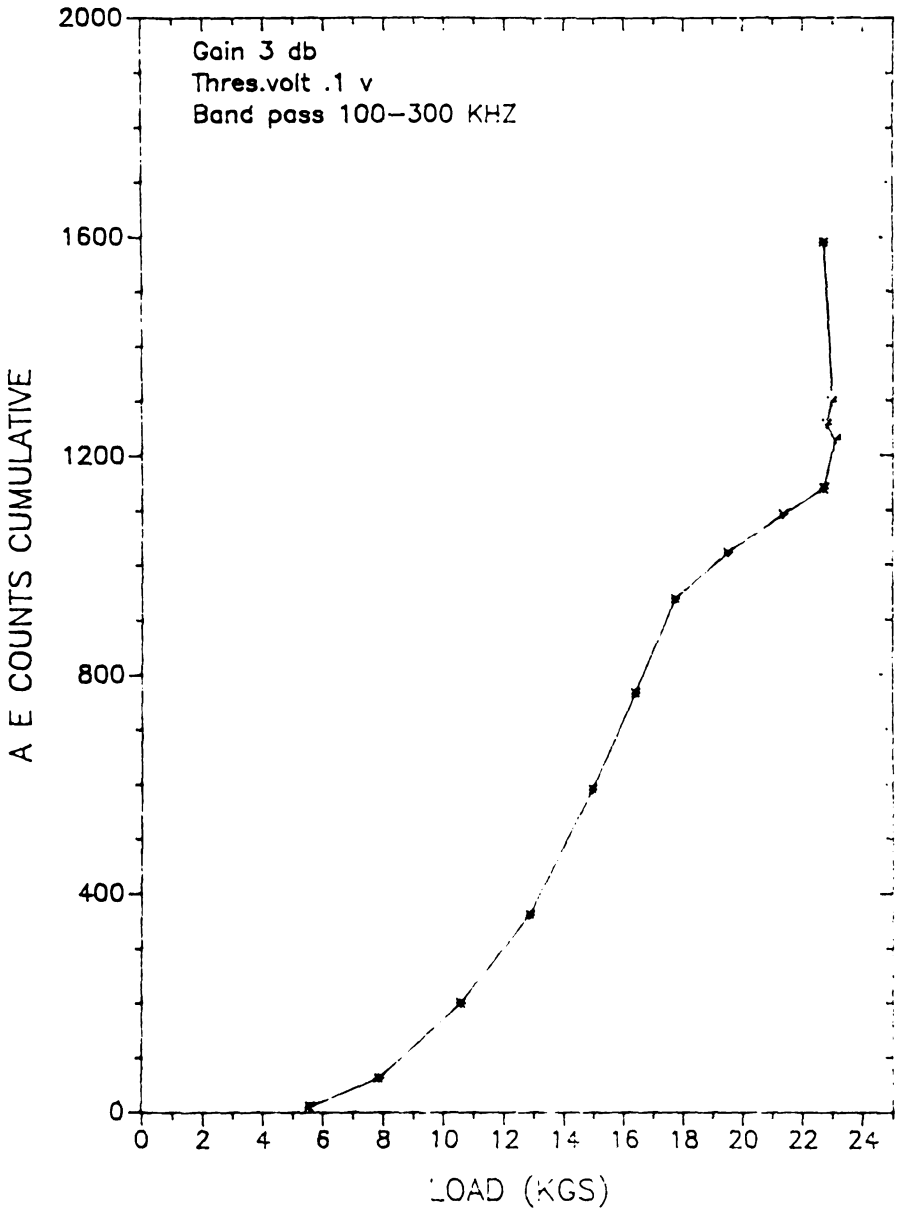

FIG.26. AE counts-load plot for tension test of symmetric Cu-Ni-Cu composite specimen annealed at 800 ^{o} C for 35 minutes

FIG
ten
an

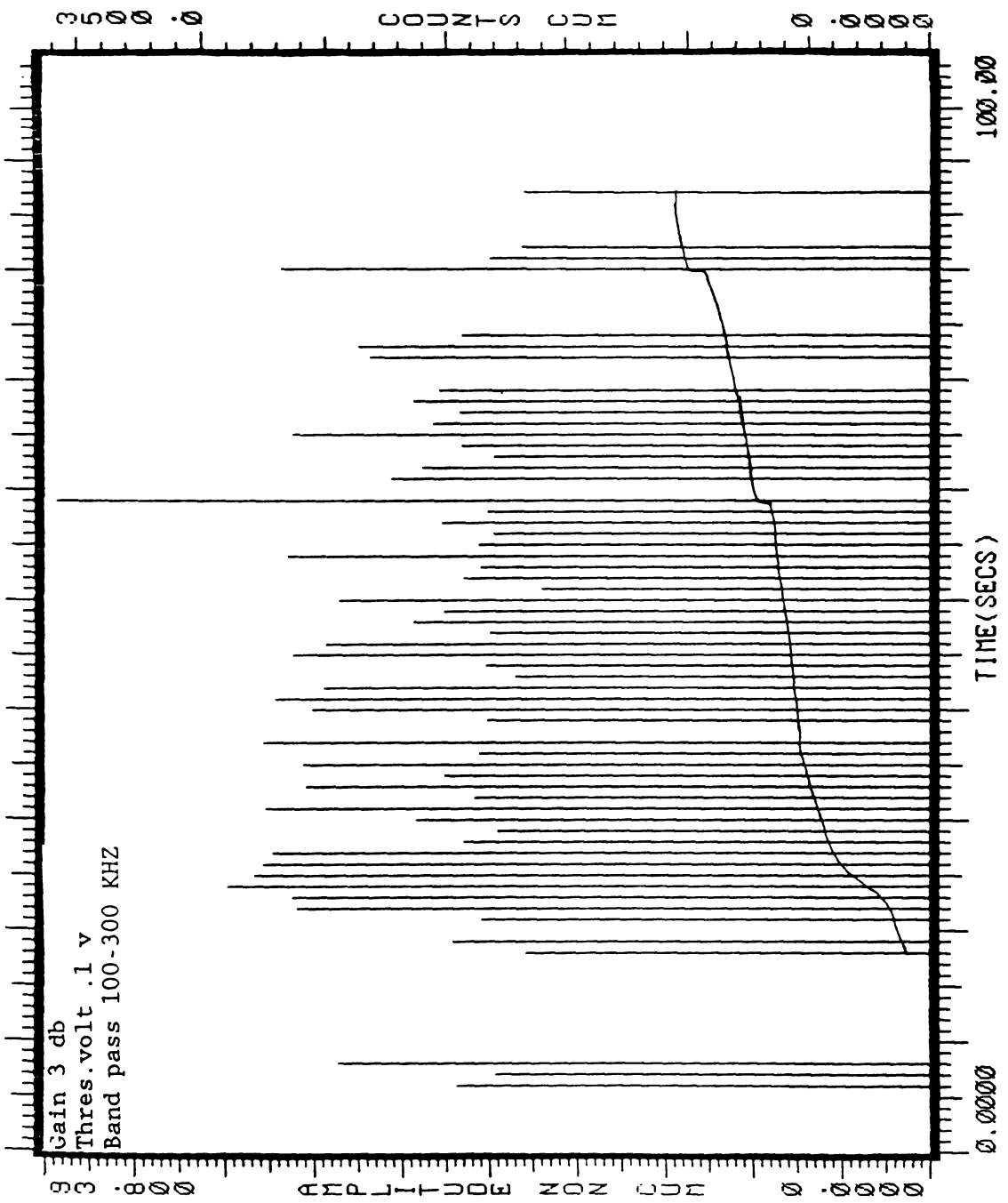

FIG.27. Joint AE counts-time and AE amplitudetime curve for tension test of sysmmetric(Cu-Ni-Cu) composite specimen annealed at 800 ^{0} C for 60 minutes.

curve th

increase

on Fig.2

Fig

800°C. T

specime

burned s

near th

of tota

emitte

shows A

Fi

the ter

minute

from t

the AE

for th

descri

I

speci

inter

seen

lot o

acous

tensi

abov

at

curve the slope is very high. That shows a high rate of stress increase at two spots during tension. The same phenomenon can be seen on Fig.28.

Fig.29 is from a symmetric composite annealed for 120 minutes at 800°C. The rate of AE counts is very high compared to the previous specimen. Actually this specimen was burnt during annealing. That burned spot acted like a notch (stress concentrator) and the region near the spot yielded quickly. This is specimen had the highest number of total AE counts of all the annealed specimens. This specimen emitted AE emission of higher amplitude throughout the test. Fig.30 shows AE counts-load plot for this specimen.

Fig.31 is the joint AE counts-time and amplitude-time curve for the tension test of a symmetric composite specimen annealed for 180 minutes at 800°C. This specimen also had voids at the interface (seen from the SEM micrograph, Fig.38), thus the bonding wasn't good and the AE activity started quite early. Fig.32 shows AE counts-load plot for this specimen. Fig.33 shows AE counts-load plot for all specimens described previously.

Figs. 34-38 show the SEM picture of the fracture surface of the specimens described above. Clear delamination can be seen at the interface in Figs. 34,35 and 36. In Fig.36 some fused metal can be seen hanging. Figs. 37 and 38 show fused metal at the interface with a lot of voids. These voids were responsible for the the increased acoustic emission from the composite specimens at a lower load during tension test.

Figs. 39-43 show the composition profile of the interface for the above specimens. There was variation in the size of the diffusion zone at the interface. Also since these composition profiles were obtained


A.E. COUNTS CUMULATIVE

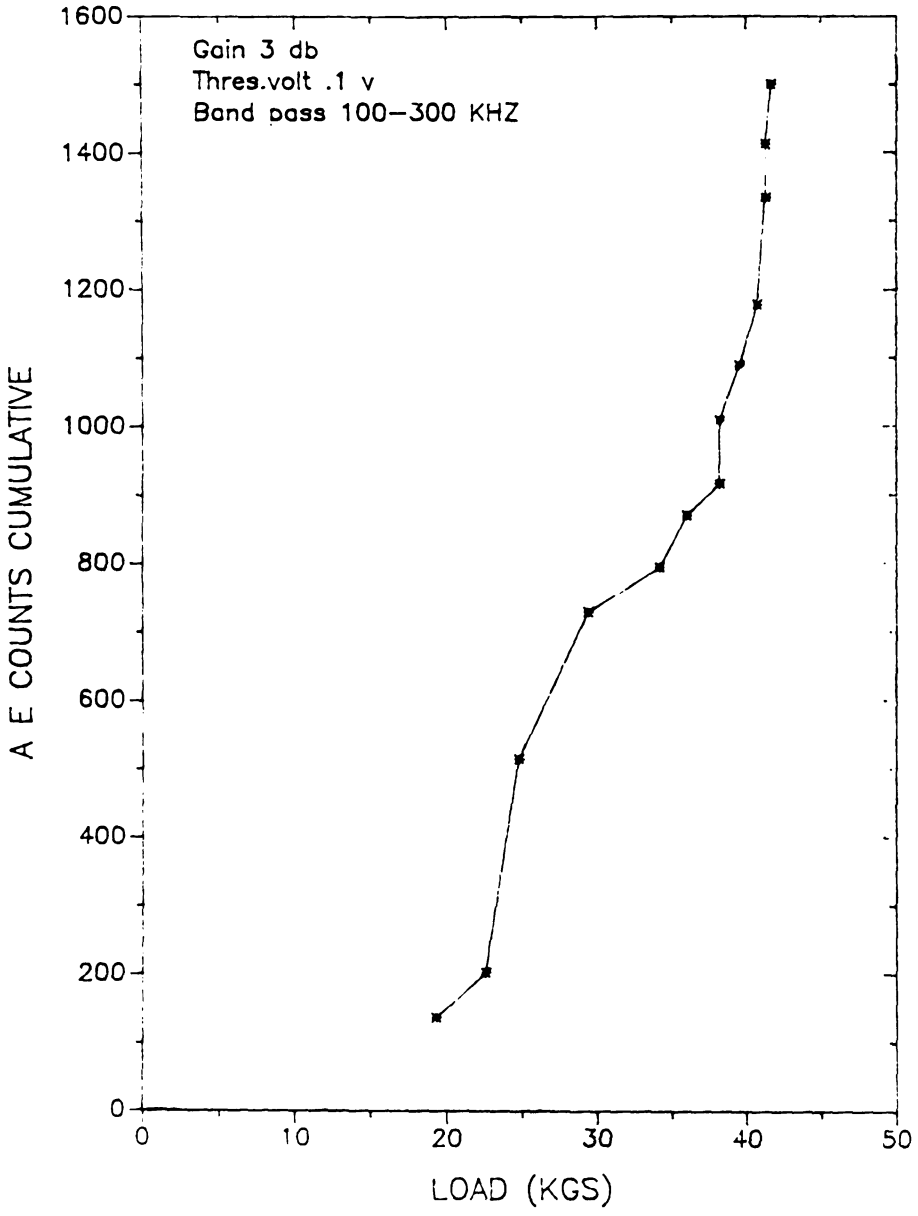

FIG.28. AE counts-load plot for tension test of symmetric Cu-Ni-Cu composite specimen annealed at 800 ^{o} C for 60 minutes

FI
te

a

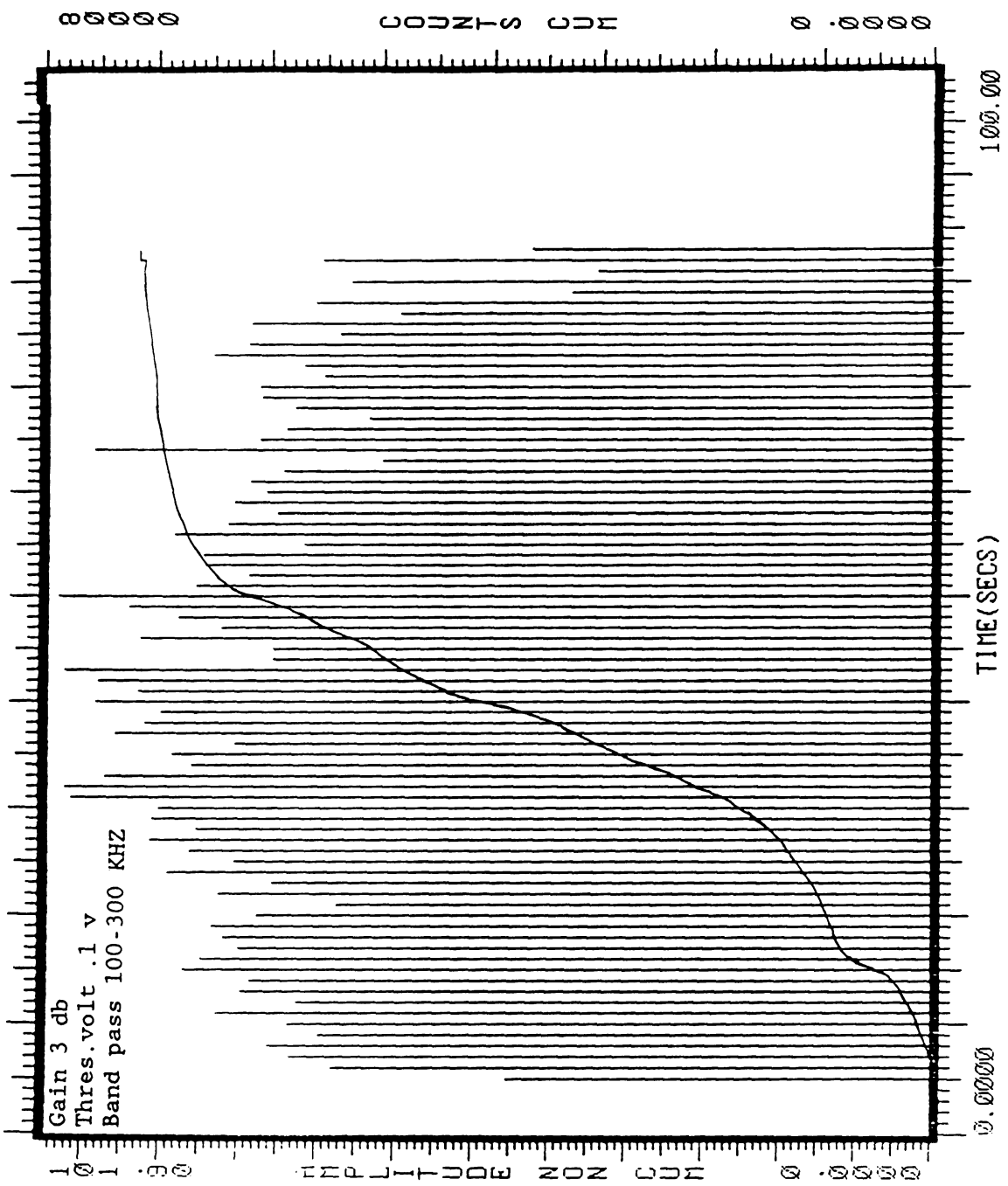

FIG.29. Joint AE counts-time and AE amplitudetime curve for tension test of sysmmetric(Cu-Ni-Cu) composite specimen annealed at 800 ^{0} C for 120 minutes.

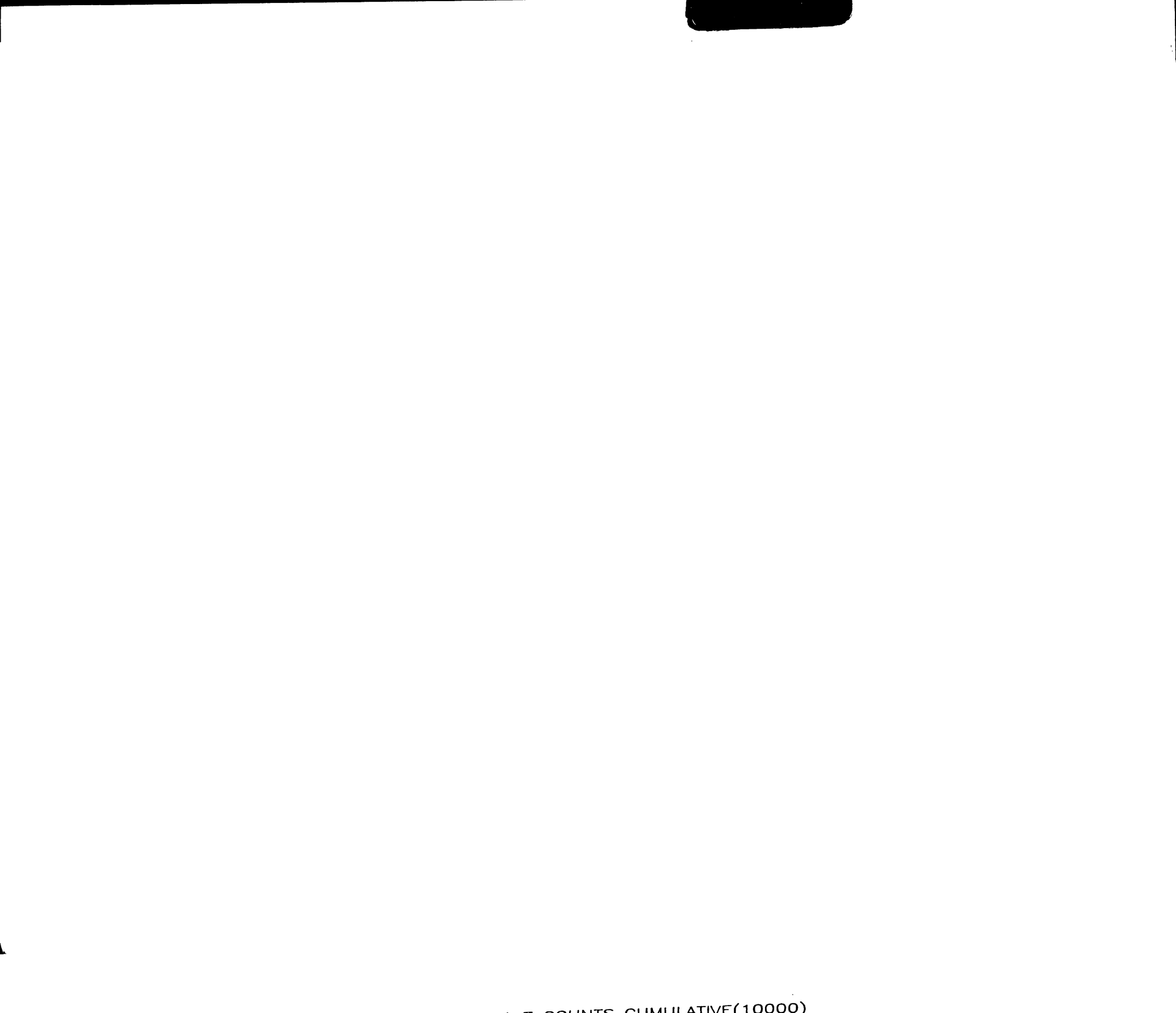
COUNTS CUMULATIVE(10000)

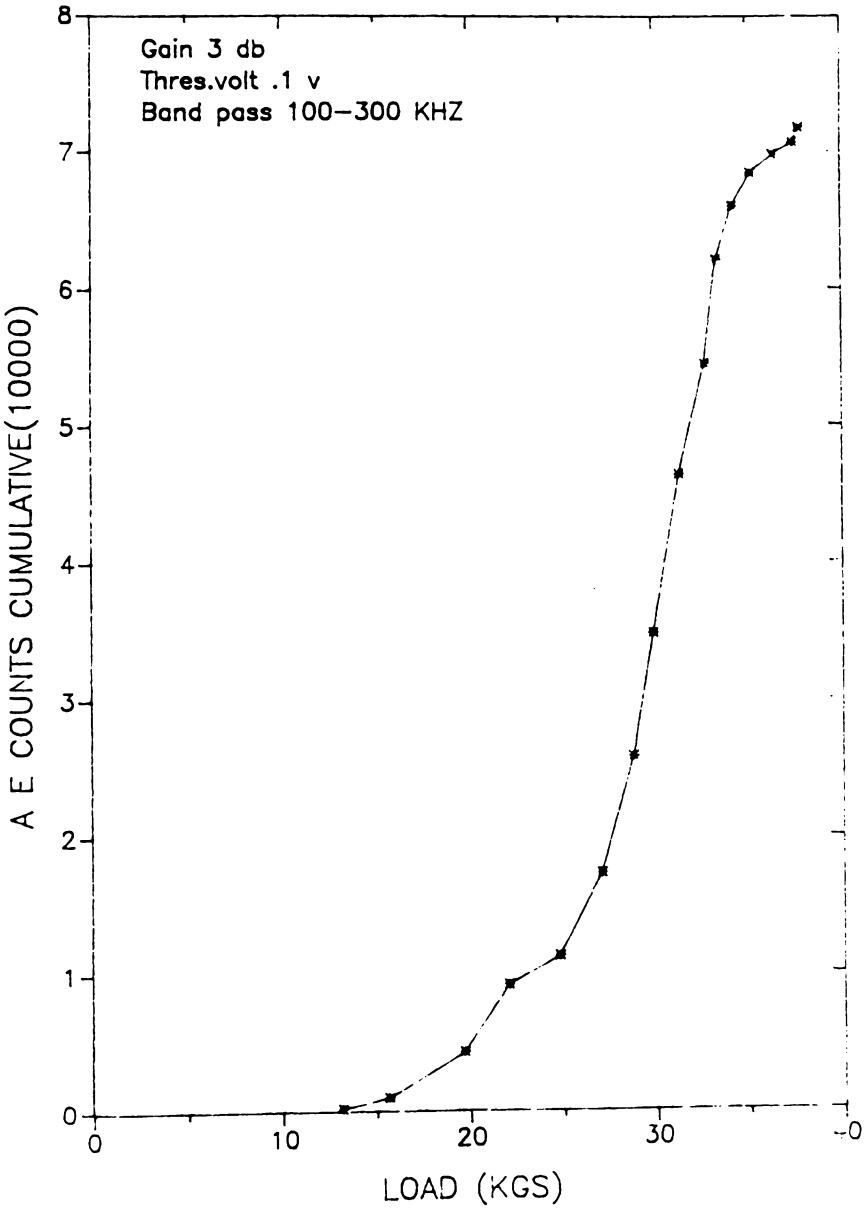

FIG.30. AE counts-load plot for tension test of symmetric Cu-Ni-Cu composite specimen annealed at 800 ^{o} C for 120 minutes


Gain 3 db

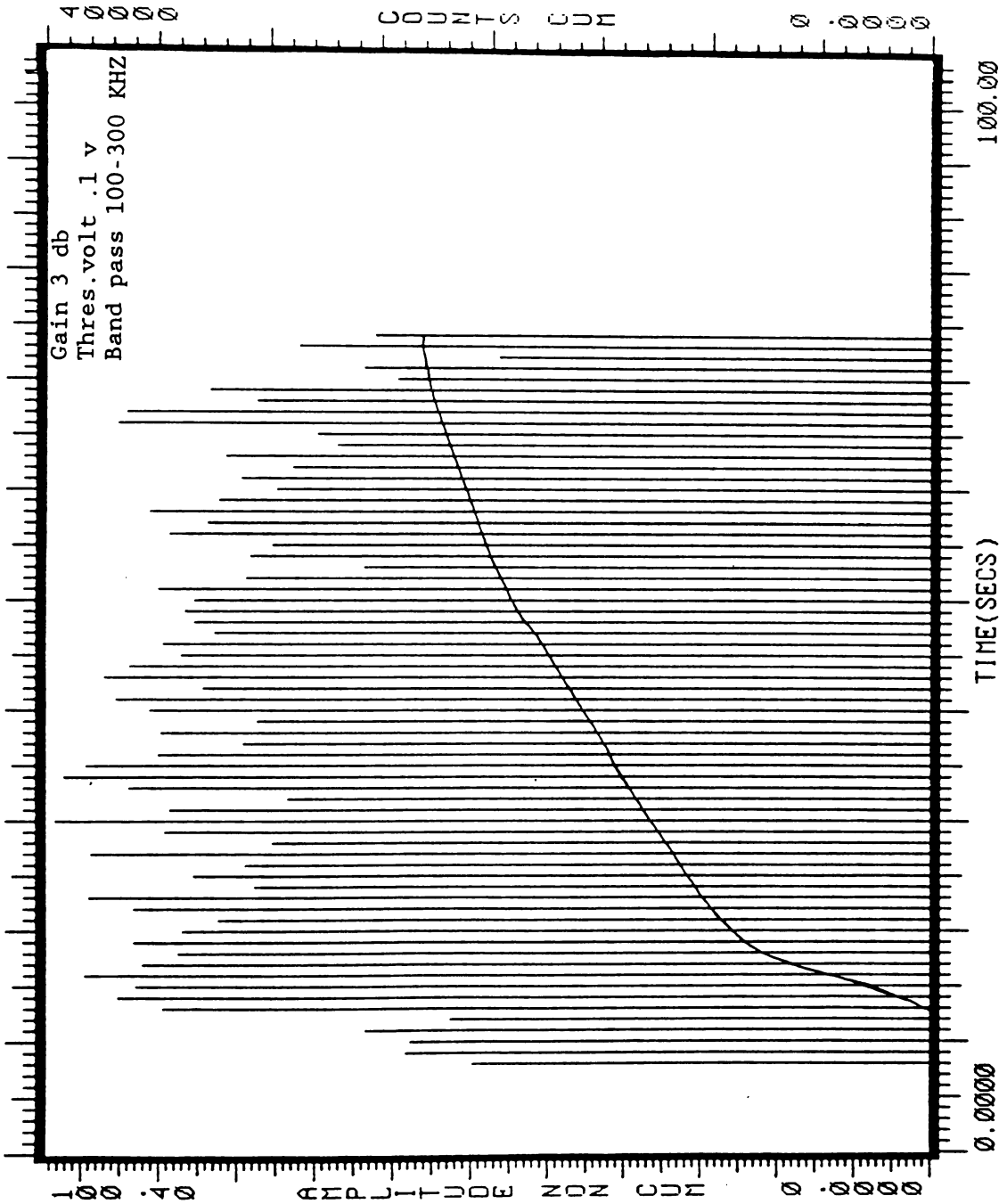

FIG.31. Joint AE counts-time and AE amplitudetime curve for tension test of sysmmetric(Cu-Ni-Cu) composite specimen annealed at 800 ^{0} C for 180 minutes.

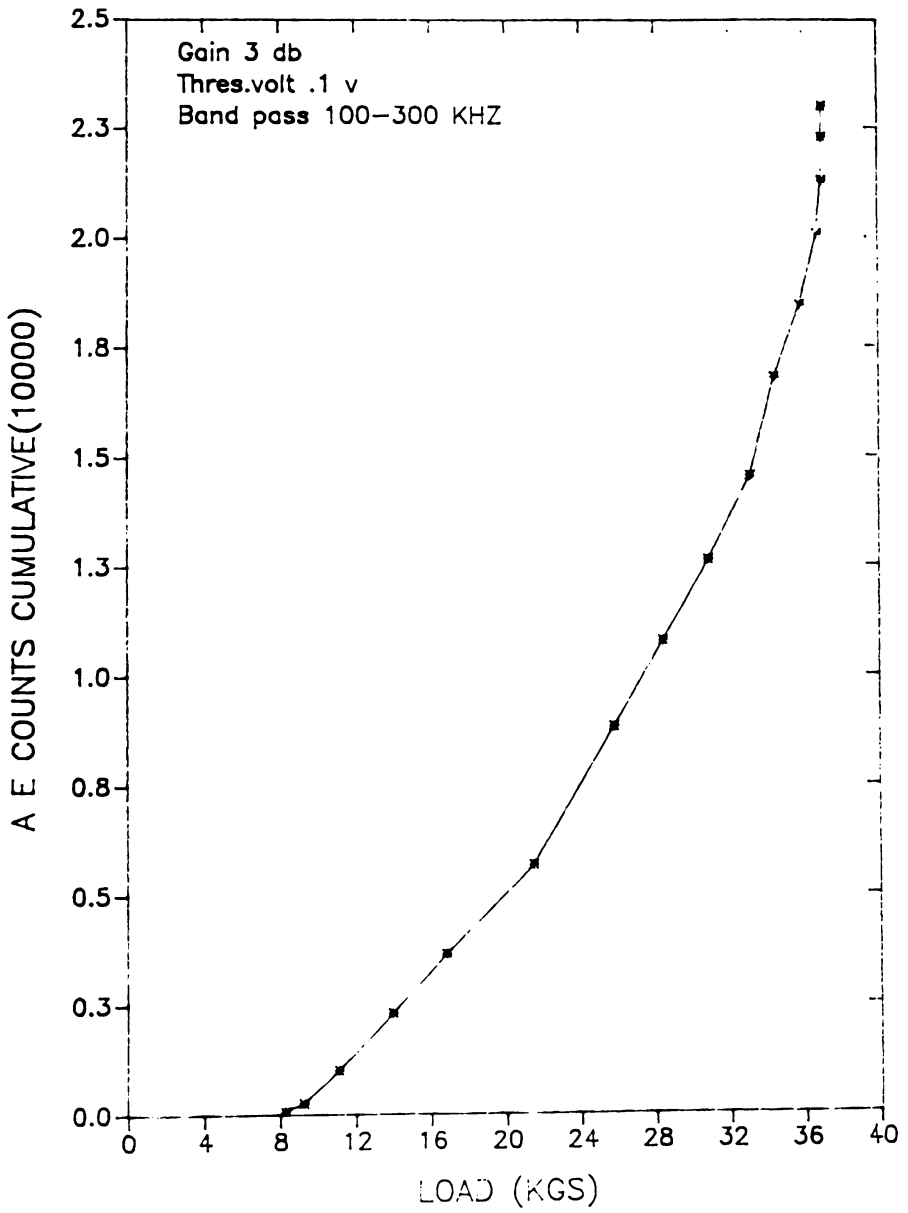

FIG.32. AE counts-load plot for tension test of symmetric Cu-Ni-Cu composite specimen annealed at 800 ^{o} C for 180 minutes

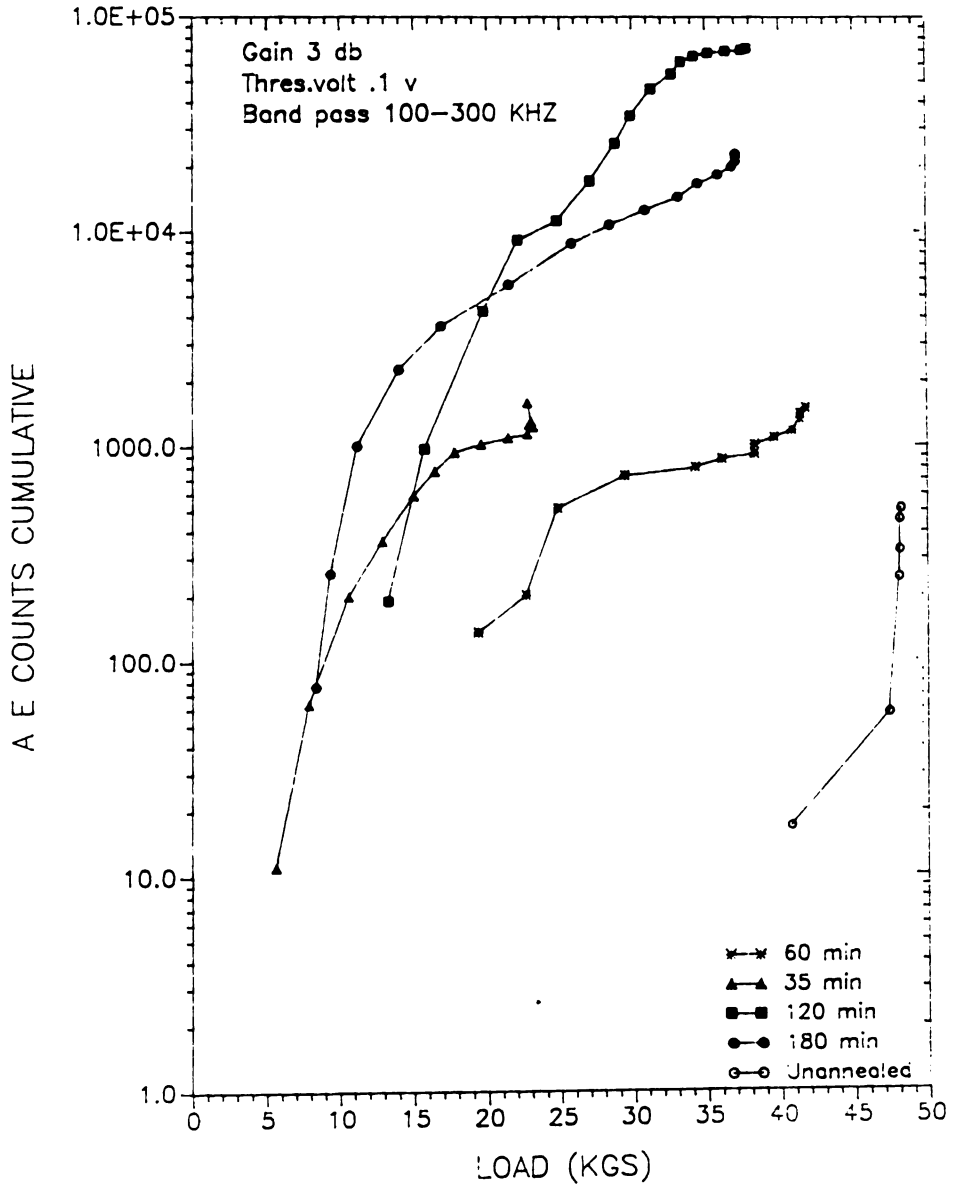

FIG.33. Comparison of AE counts-load for tension test of symmetric (Cu-Ni-Cu) composite specimens annealed at 800 C for different duration.

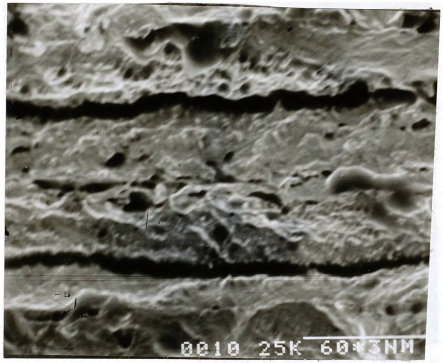

FIG.34. SEM micrograph of fracture surface of symmetric Cu-Ni-Cu composite (unannealed) tensile specimen.

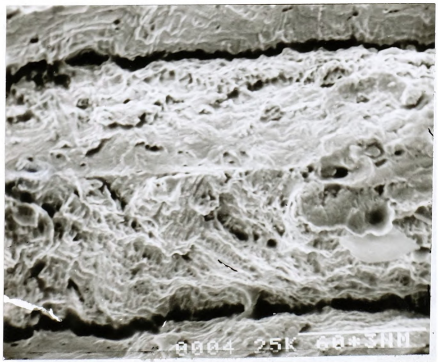

FIG.35. SEM micrograph of fracture surface of symmetric Cu-Ni-Cu composite tensile specimen, annealed at 800°C for 35 min.

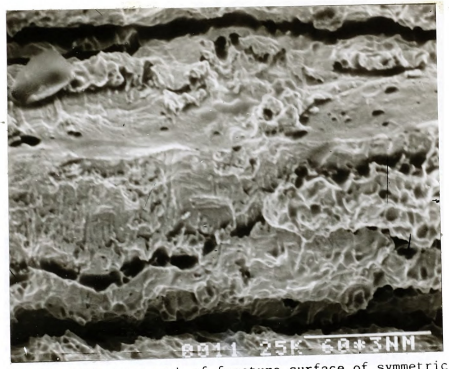

FIG.36. SEM micrograph of fracture surface of symmetric Cu-Ni-Cu composite tensile specimen,annealed at 800°C for 60 min.

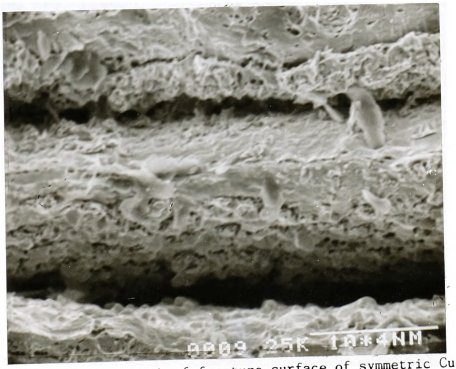

FIG.37. SEM micrograph of fracture surface of symmetric Cu-Ni-Cu composite tensile specimen, annealed at 800°C for 120 min.

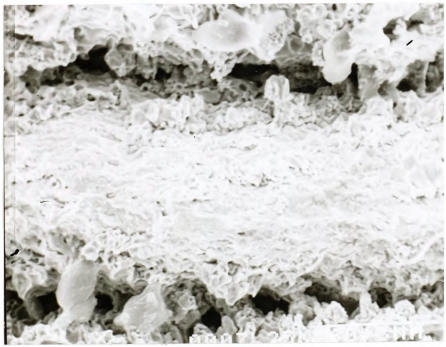

FIG.38. SEM micrograph of the fracture surface of symmetric Cu-Ni-Cu composite tensile specimen, annealed at 800°C for 180 minutes.

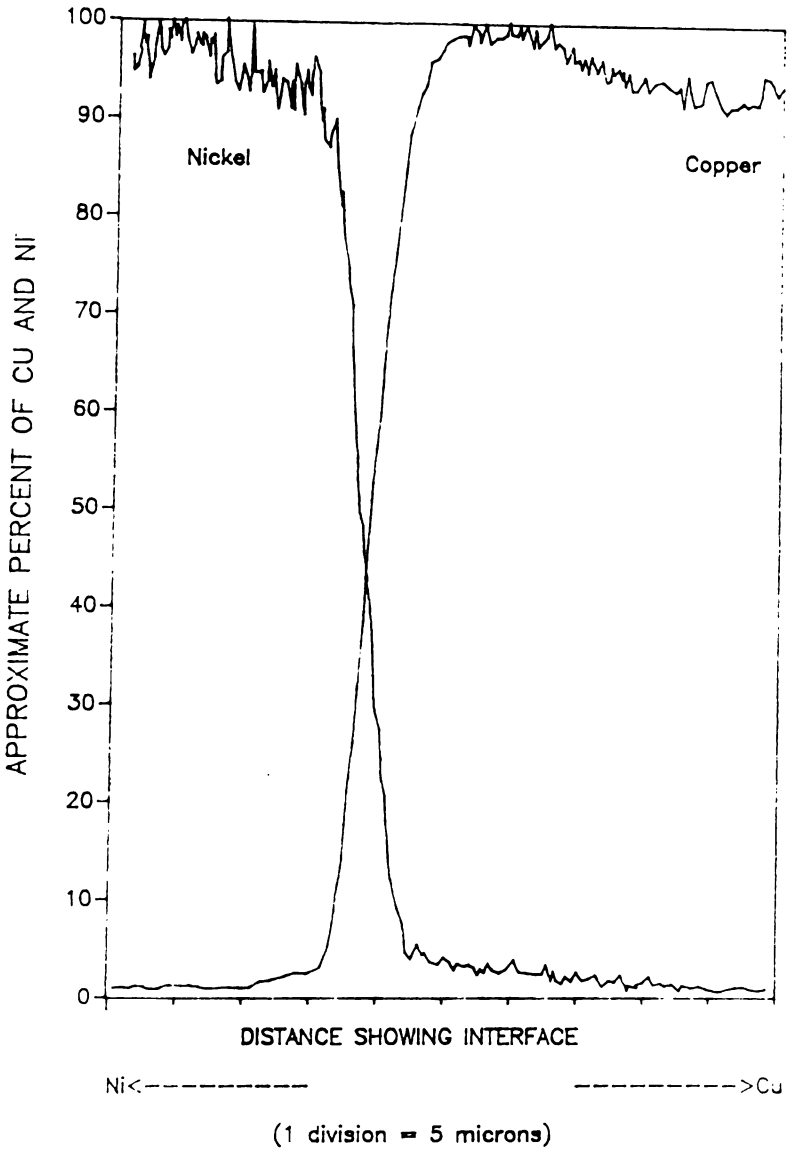

FIG.39. Composition profile of interface of symmetric(Cu-Ni-Cu) unannealed composite specimen.

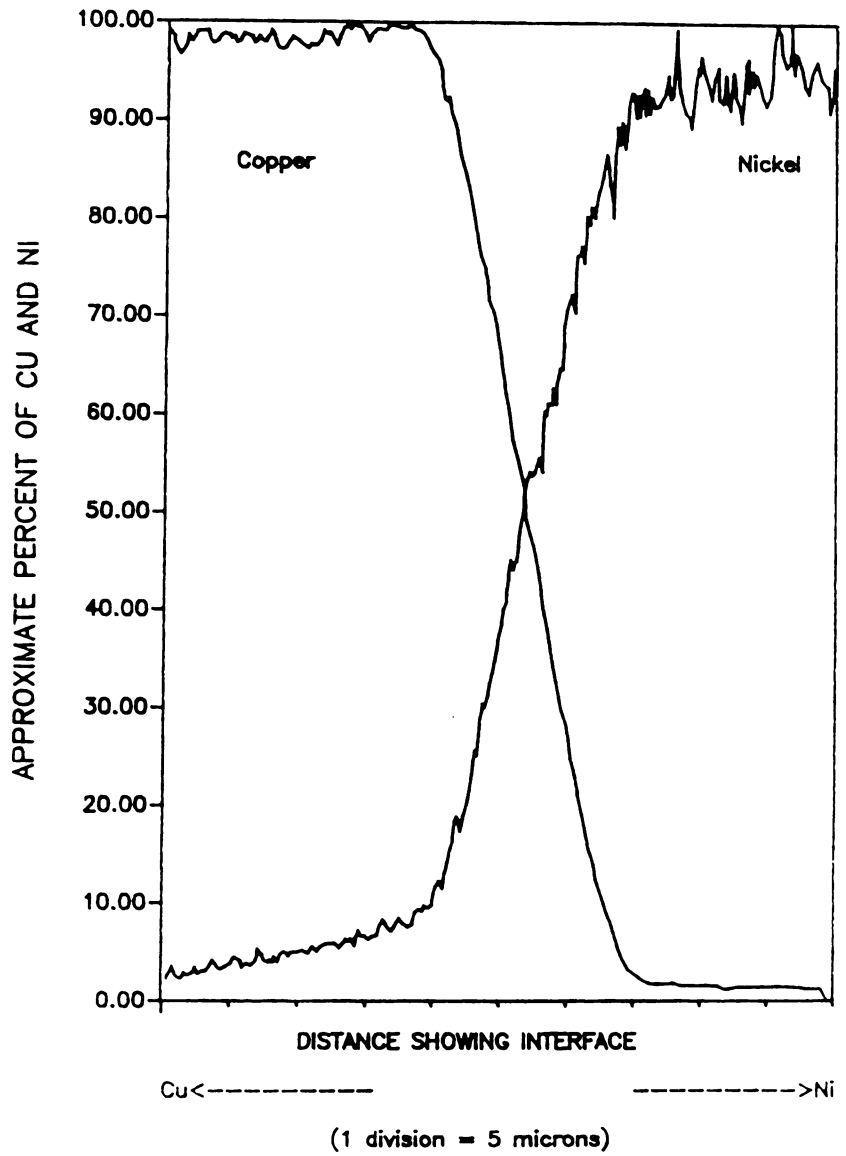

FIG.40.Composition profile of interface of symmetric(Cu-Ni-Cu) composite specimen annealed at 800 C for 35 minutes.

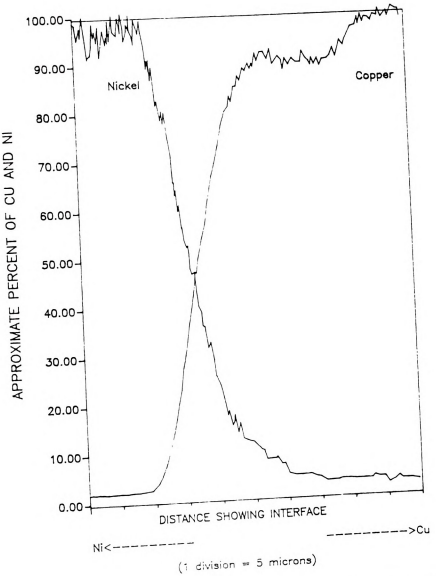

FIG.41. Composition profile of interface of symmetric(Cu-Ni-Cu) composite specimen annealed at 800 C for 60 minutes.

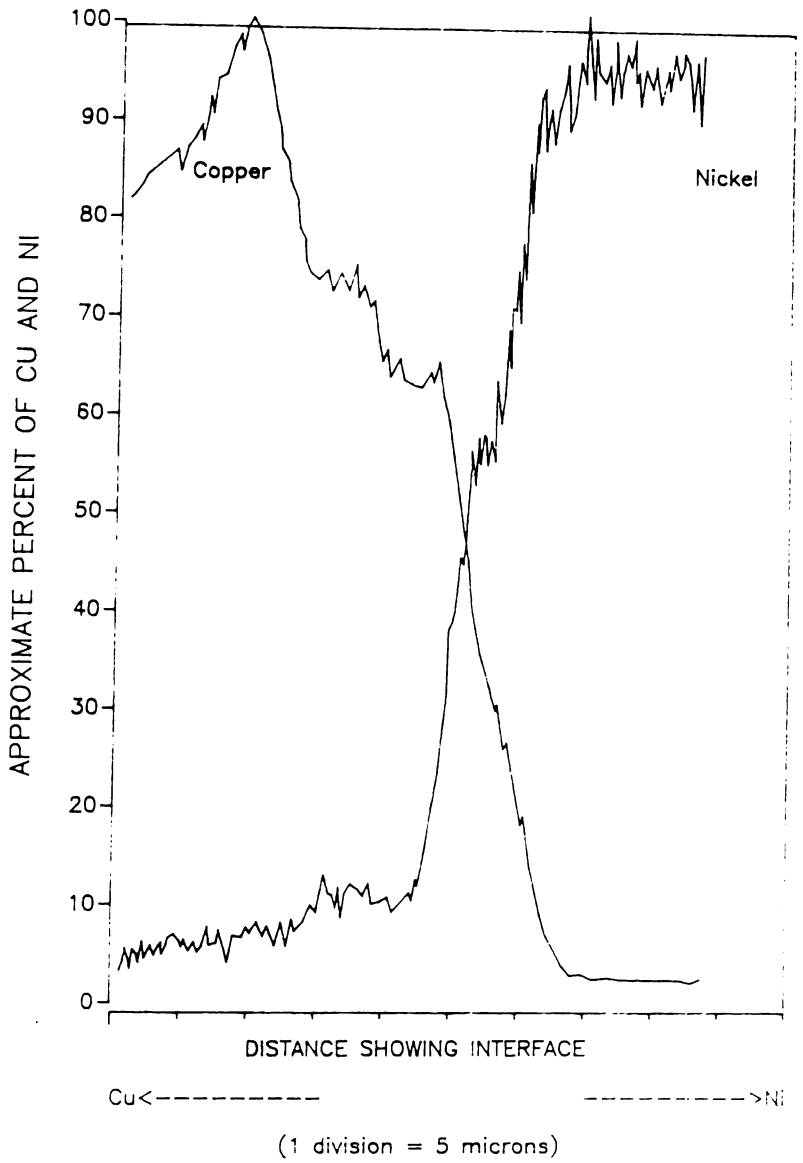

FIG.42. Composition profile of interface of symmetric(Cu-Ni-Cu) composite specimen annealed at 800 C for 120 minutes.

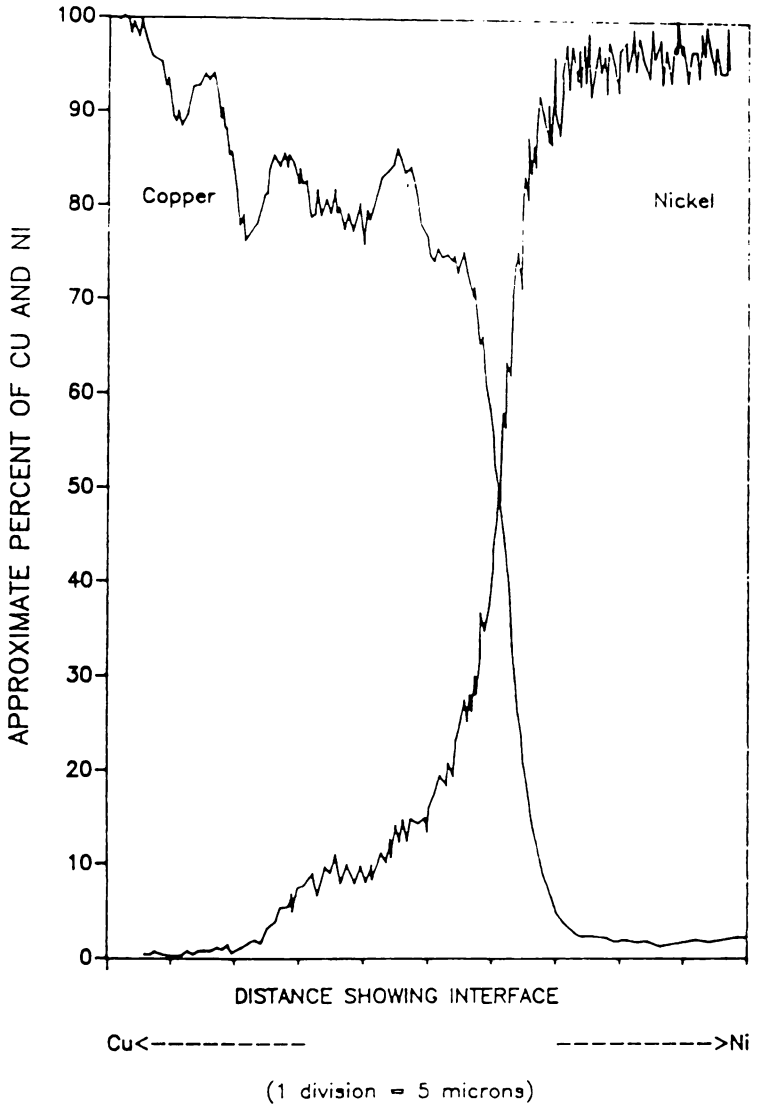

FIG.43. Composition profile of interface of symmetric(Cu-Ni-Cu) composite specimen annealed at 800 C for 180 minutes.

from the failed specimens from tension, the presence of cracks also affected the data. For example Fig.45 shows the presence of a crack clearly. In general, a broadening of the solute distribution at the interface and a region of relatively constant solute concentration (i.e plateau) throughout the remainder of the composite is observed from the composition profiles. The slight interfacial broadening exhibited by the unannealed composite is due primarily to insufficient resolution by the electron microprobe. Table 3 summarises the different parameters for the above specimens.

TABLE 3 UTS, total AE counts and diffusion width.

Annealing time at 800 C	Zone width (micron)	AE counts (ΣN)	UTS (kg/sq mm)
0(unannealed)	7.125	500	38.06
35 min	10,9.75	1600	19.81
60 min	17	1550	35.08
120 min	38.5,28.5	80000	31.64
180 min	32	25000	31.7

Figs. 44 and 45 show pictorial representation of tensile specimens with artificial defects of different sizes. All specimens in each set were made from the same composite plate (made under the same conditions of electroplating). Fig.46 shows the AE response of the defective specimens 1,2,3 (set A) to the tension test. From this figure it is evident that, as the size of the defect increased, the acoustic emission counts increased. The slope of the AE counts-time curve for specimen with bigger size defect (shape same) is higher than the one for specimen with smaller size defect. But we cannot

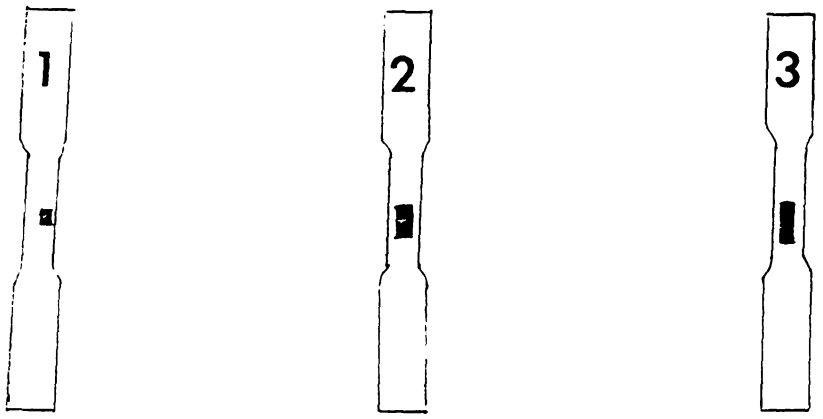

FIG.44. Three different symmetric Cu-Ni-Cu composite tension specimens with defects (varying size) at one of the interface.All from One composite plate (Set A).

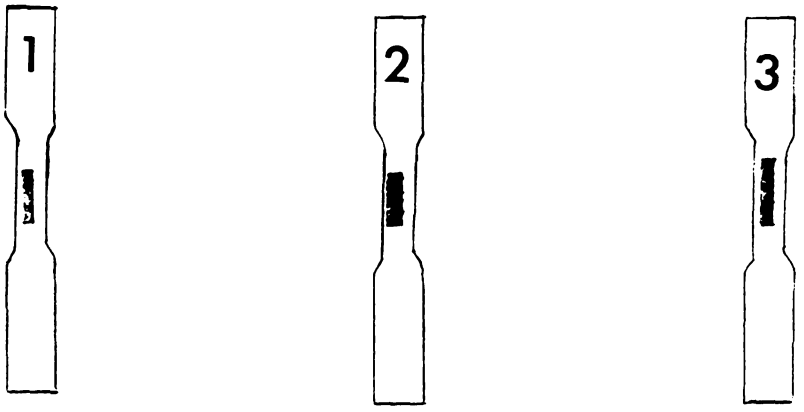

FIG.45. Three different symmetric Cu-Ni-Cu composite tension specimens with defects(varying size) at one of the interface.All from one composite plate (Set B)

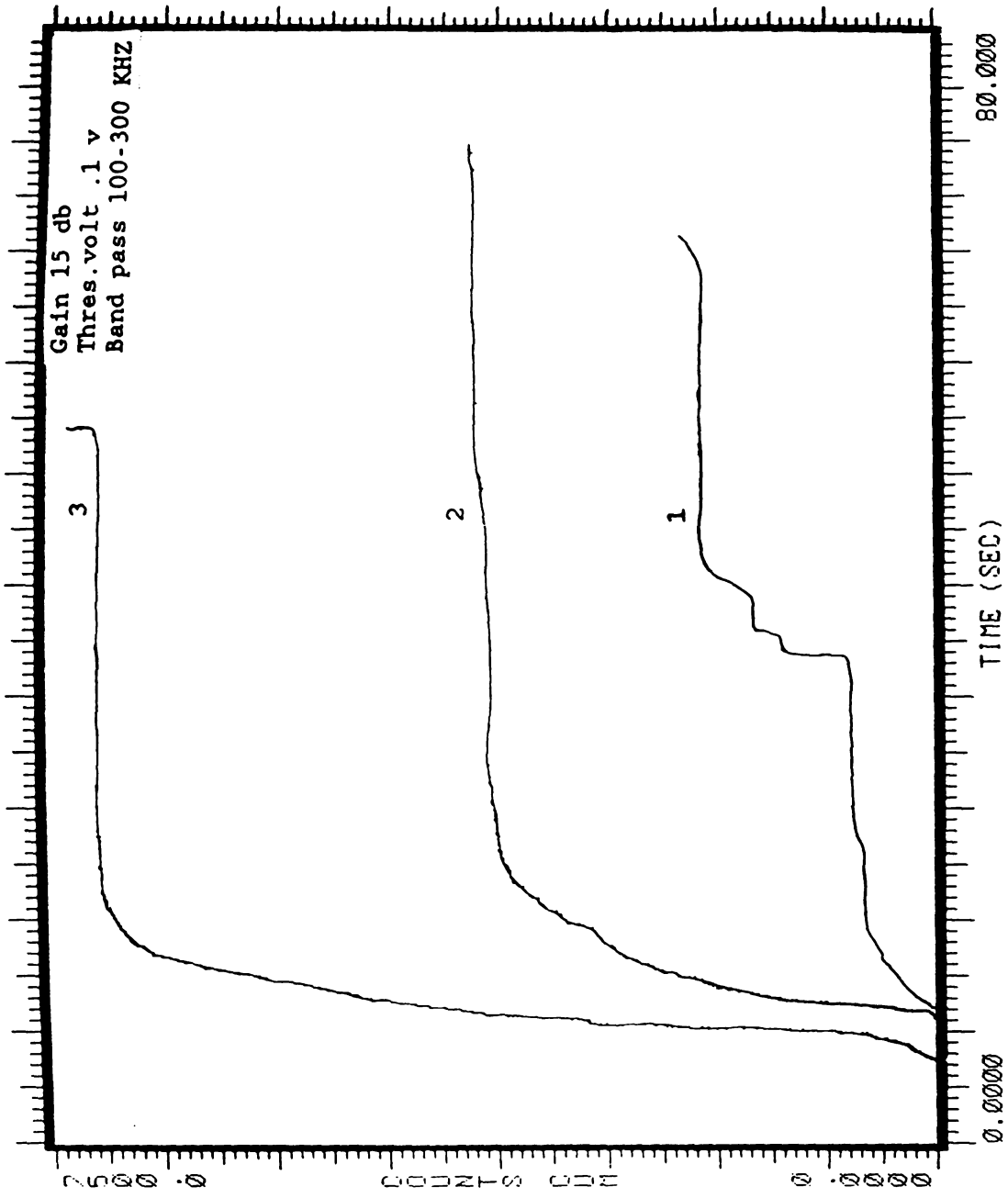

FIG.46. Comparison of AE counts-time for tension test for specimens from set A, having voids (of varying size).

generalise the fact, since acoustic emission in a specimen containing a defect, stressed below general yield is dependent on plastic strains in the vicinity of the defect sides and these strains in turn depend on stress intensity factors. Stress intensity factors depend on the sample geometry, the shape ,size and location of the flaw and the type of loading [37]. In our case all of these factors were common for all specimens except the size of the defect, so we can infer that their AE characteristics are closely related to stress intensity factors for the defect present. Fig.47 shows the AE counts-time plot for the specimens 1,2,3 of set B. This plot is in consistant with the result obtained for the specimens of set A. Fig.49 shows the x-radiograph of the plated composite plate with defects (Specimens of set B were made from this composite plate).

Fig.48 illustrates the validity of the Kaiser effect [38]. One asymmetric composite tensile specimen was pulled to a load, just greater than the yield point and unloaded completely. It was then pulled again until failure. AE data was recorded during both parts of the test (initial loading and reloading). Fig.48 shows that no acoustic emission was emitted until the load exceeded the previous load. During reloading the previous load was reached in 2.5 seconds (shown in load-time curve) and no acoustic activity was recorded during these 2.5 seconds. Two other specimens were also tested to establish the Kaiser effect for copper-nickel composites.

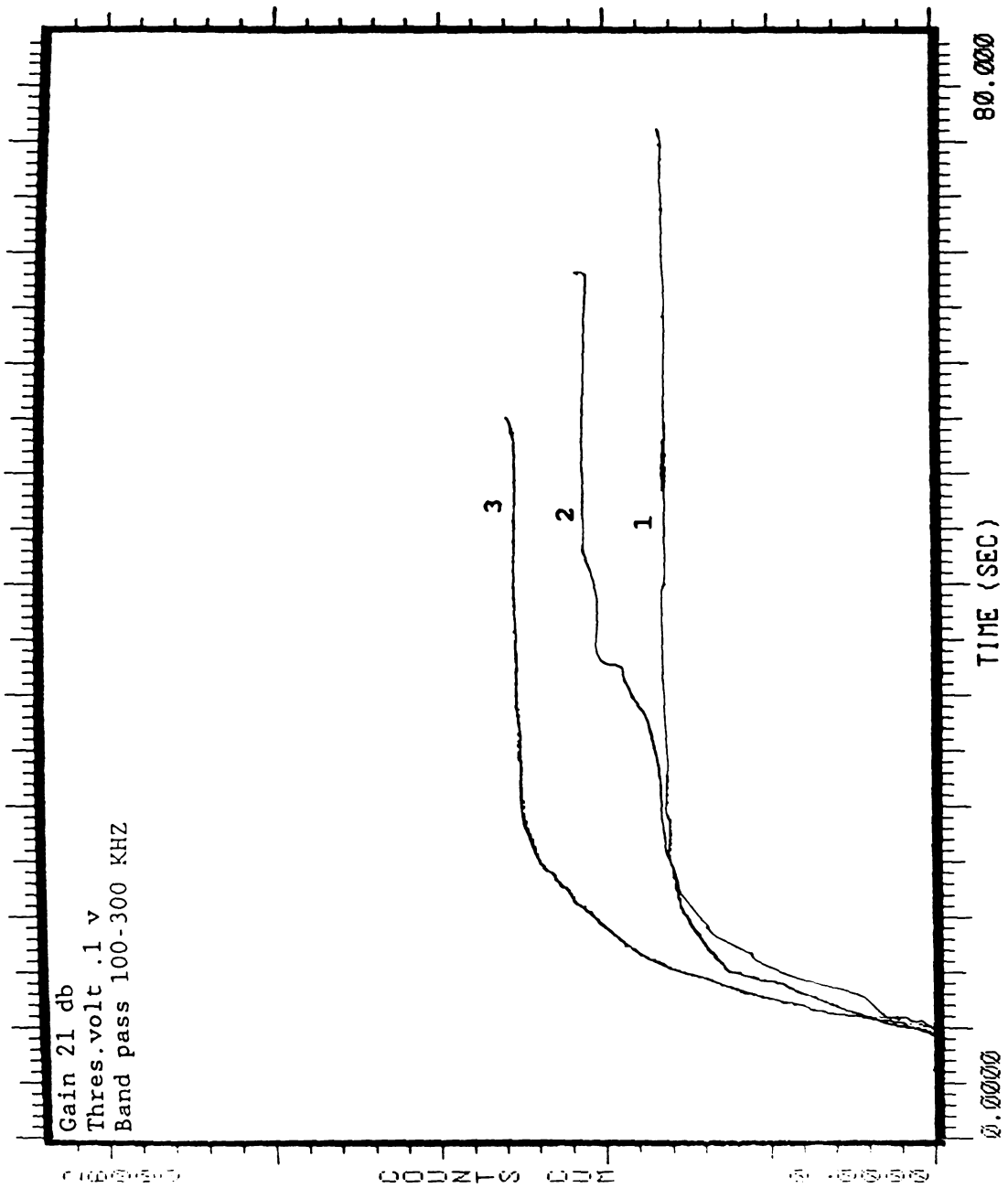

FIG.47. Comparison of AE counts-time for tension test of specimens from set B, having voids (of varying size).

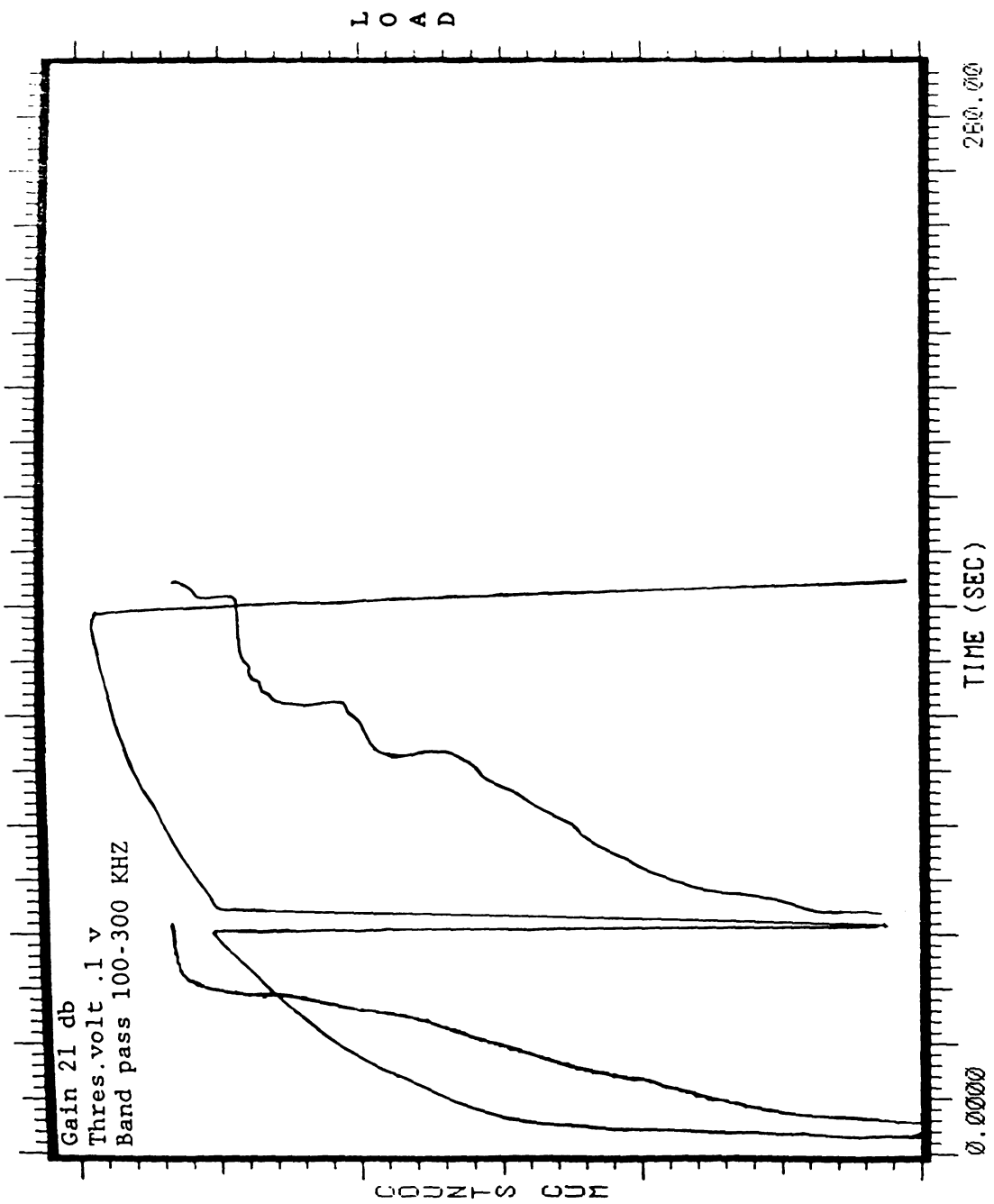

FIG.48. AE counts-time and load-time curve for tension test of asymmetric(Cu-Ni) composite specimen showing Kaiser effect.

FIG.49. X radiograph of a symmetric composite plate,showing voids. (specimens of set B were made from this plate)

V. CONCLUSIONS

In this research the mechanical response of copper-nickel metallic composites to tensile loading was studied. Acoustic emission testing, SEM and electron microprobe analysis were used for investigation of cracking interface structure and interface chemistry respectively. The following conclusions were made:

(1) Annealing of these composites produces a broadening of the solute distribution at the interface and a region of relatively constant solute concentration through-out the remainder of the composite.

(2) Acoustic emission signals can be used to characterize the mechanical response of these composite. The slope of the acoustic emission counts-time curve represents rate at which plastic yielding is going on, in the vicinity of the defect. In composites with perfect bonding (no defect) the AE activity will be greatest just before general yielding (during transition).

(3) Stress intensity factors at the defect controls plastic yielding, which in turn controls the acoustic emission from the specimen under load. This relationship of stress intensity factor and acoustic emission can be utilised to predict the integrity of metallic composites.

(4) Since the Kaiser effect is valid for metallic composite, it may be used to predict the integrity of metallic composites.

(5) Acoustic emission can be used to evaluate bonding in metallic composites. Acoustic emission activity, during loading, starts very early in the presence of a bad bond (below the yield point). At any given load, the number of cumulative AE counts is higher for a bad bond than for a good bond.

REFERENCES

1. Albert, Hoersch jr, Composite Engineering Laminates, Editor Albert, G. H, Cambridge, MIT press(1969).
2. Altiero, N.J, Fink, F.T, Mukherjee, k., Proposal submitted to the centre of composite and structures, MSU (Unpublished) (1984).
3. Iron Age, July 31, 1978, p.93.
4. Raymond, J.L, Iron Age, Feb.12, 1979, p.84.
5. Koehler, J.S , Physical Review B ,Vol 2 , No. 2 ,July 1970, p.547.
6. Lehoczky, S.L , J. Appl. Phys; Vol 49 , No. 11, Nov.1978, P.5474.
7. Yoshi, K., Takagi, H., Umeno, M., Met. Trans. A, Vol 15A, June 1984, p.1275.
8. Morgan, J.B., Composite Engineering Laminates, Chap 12, Editor Albert, G.H, Cambridge, MIT press(1969).
9. Cohen, U., Koch, F.B., Sard, R., J. Electrochem. Soc. Vol 130 , No.1, p.1987 (1983).
10. Blum, W., Trans. Am. Electrochem. Soc.,40 , 307 (1921).
11. Henning, C.A.O., Boswell, F.W., Corbett, J.M., Acta met. Vol 23, Feb.1975, p.177.
12. Henning, C.A.O., Boswell, F.W., Corbett, J.M., Acta met. Vol 23, Feb.1975, p.187.
13. Semiatin, S.L., Piehler, H.R., Met. Trans. A, Vol 11A, p.85, (1979).
14. Johnson, B.C., Bauer C.L., Jordan, A. G., J. Appl.Phys., Vol 9, No.4, p.1147 (1986).
15. Tenney, D.R., Carpenter, J.A., Houska, C.R., J. Appl. Phys. Vol 41, No. 11, p.4486 (1986).

16. Gdoutos, E.E., Problems of mixed mode crack propagation, Chap.7, p.137 (1984).

17. Semiatin, S.L., Piehler, H.R., Met. Trans. A, Vol 10A, p.1107 , (1979).

18. Da Silva, L.C.C., Mehl,R.F, Transactions AIME, Vol 191, p.155, (1951).

19. Dor-Ram, J., Weiss, B.Z., Kohen, y., Met. Trans. A, Vol 8A, p.518, (1951).

20. Wadley, H.N.G., Scruby, C.B., Speake, J.H., International Met. Reviews, No.2, p.41 (1980).

21. Drovillard, T.F., Liptai, R.G., Tatro, C.A., Monitoring structural integrity by acoustic emission (1975).

22. Speich, G.R., Fisher, R.M., Acoustic emission, ASTM STP 505, (1972)

23. Williams, R.V., Acoustic emission, Adam Higler Ltd,Bristol, P.88 (1980).

24. Morais, C.F., Green, A.T., ASTM STP 571, p184 (1975).

25. Liptai, R.G., Horris, D.O., Tatro, C.A., ASTM STP 505, p.3.

26. Manual for 3000-3004 PAC AE system, Physical acoustic corporation (1975).

27. Pollock, A.A., Acoustics and vibration progress , Editors R. stephens and H. leventhol.

28. Ono, K., Mat. Evaluation, Aug 1976, 34, p.177.

29. Tatro, C.A., Acoustic emission, ASTM STP 505 , p.84 (1972).

30. Sharpe, R.S., Resesearch Techniques in NDT, p.12 (1970).

31. Graham, L.J., Alers, G.A., Mater. Evaluation, Feb. 1975 ,32, p.31.

32. Bossim, M.N., Hussny-Ema, M., Acoustic emission ,edited by James R. Mathews,Gordon and Breach sci. publishers (1983).

33. Tatro, C.A., Brown, A.E., Freeman, T.H., Yanes, G.U., Acoustic emission monitoring of pressurized system, p.70, (edited by Hartman/Mcelrony),ASTM STP 697 (1979).

34. Dunegan, H.L., Greene, A.T., ASTM STP 505 , p.106 (1972).

35. Hamstad, M.A., Chiao., T.T., Composite reliability, ASTM, p.191 (1984).

36. Dunegan, H.L., Harris, D.O., Tatro, C.A., Eng. Fract. Mech. J. Vol 1, ASME, p.387 (1968).

37. Dunegan, H.L., Feb. 1975, Met. Engineering quarterly ,p.8.

38. Mathews, J.R., Hay, D.R., Acoustic emission evaluation, Gordon and Breach Publishers, p.1 (1983).

39. Metal finsihing , Guidebook Directory, Metals and plastics publications,Inc. NY (1985).

40. Blum, W., Hogaboom, G.B., Principles of electroplating and electroforming.

41. Rose, J.l., Shelton, W., Composite reliability , ASTM STP 580 , p.215 (1975).

42. Chang, F.H., Couchman, J.C., Composite reliability, ASTM STP 580, p.177 (1975).

43. Pisarenko Et al, G.S., Mechanics of nondestructive testing (edited by W.W. Stinchkomb),Plenum press,NY, p.367 (1980).